



US ARMY
MATERIEL
COMMAND

12

AD F50076

MEMORANDUM REPORT BRL-MR-3523

AD-A171 462

DRAG PREDICTIONS FOR PROJECTILES AT
TRANSONIC AND SUPERSONIC SPEEDS

Jubaraj Sahu

June 1986

DTIC
SELECTED
JUL 18 1986
S
A

DTIC FILE COPY

APPROVED FOR PUBLIC RELEASE; DISTRIBUTION UNLIMITED.

US ARMY BALLISTIC RESEARCH LABORATORY
ABERDEEN PROVING GROUND, MARYLAND

86 7 18 005

Destroy this report when it is no longer needed.
Do not return it to the originator.

Additional copies of this report may be obtained
from the National Technical Information Service,
U. S. Department of Commerce, Springfield, Virginia
22161.

The findings in this report are not to be construed as an official
Department of the Army position, unless so designated by other
authorized documents.

The use of trade names or manufacturers' names in this report
does not constitute indorsement of any commercial product.

UNCLASSIFIED

SECURITY CLASSIFICATION OF THIS PAGE (When Data Entered)

REPORT DOCUMENTATION PAGE		READ INSTRUCTIONS BEFORE COMPLETING FORM
1. REPORT NUMBER Memorandum Report BRL-MR-3523	2. GOVT ACCESSION NO. AD-A191467	3. RECIPIENT'S CATALOG NUMBER
4. TITLE (and Subtitle) DRAG PREDICTIONS FOR PROJECTILES AT TRANSONIC AND SUPERSONIC SPEEDS	5. TYPE OF REPORT & PERIOD COVERED FINAL	
	6. PERFORMING ORG. REPORT NUMBER	
7. AUTHOR(s) Jubraj Sahu	8. CONTRACT OR GRANT NUMBER(s)	
9. PERFORMING ORGANIZATION NAME AND ADDRESS US Army Ballistic Research Laboratory ATTN: SLCBR-LF Aberdeen Proving Ground, MD 21005-5066	10. PROGRAM ELEMENT, PROJECT, TASK AREA & WORK UNIT NUMBERS RDTE 11162618AH80	
11. CONTROLLING OFFICE NAME AND ADDRESS US Army Ballistic Research Laboratory ATTN: SLCBR-DD-T Aberdeen Proving Ground, Maryland 21005-5066	12. REPORT DATE June 1986	
	13. NUMBER OF PAGES 46	
14. MONITORING AGENCY NAME & ADDRESS (if different from Controlling Office)	15. SECURITY CLASS. (of this report) Unclassified	
	15a. DECLASSIFICATION/DOWNGRADING SCHEDULE	
16. DISTRIBUTION STATEMENT (of this Report) Approved for public release, distribution unlimited		
17. DISTRIBUTION STATEMENT (of the abstract entered in Block 20, if different from Report)		
18. SUPPLEMENTARY NOTES		
19. KEY WORDS (Continue on reverse side if necessary and identify by block number) Navier-Stokes Computations Supersonic Flow Drag Components Pressure Drag Transonic Flow Viscous Drag Design Codes Base Drag		
20. ABSTRACT (Continue on reverse side if necessary and identify by block number) The breakdown of the total drag into its individual components (pressure drag, viscous drag, and base drag) is important in the preliminary design stage of shell. Design codes are available to predict the individual drag components and thus, the total drag. Typically, the total drag predicted by these design codes agrees well with the total drag measured from flight tests. But, how well do these codes predict the individual drag components? Experimental verification of the prediction of the drag components is an extremely difficult task.		

20. ABSTRACT (Continued)

Thus, a Navier-Stokes computational procedure is used in this report to predict the individual drag components and test the accuracy of the predictions of the design codes. A thin-layer Navier-Stokes code has been used to compute the entire flow field over projectiles including the base region. Numerical calculations have been made for various Mach numbers in the transonic and supersonic regimes. Pressure drag, skin friction drag, base drag and thus, the total drag are obtained from the computed results. Comparison of drag has been made with available experimental data and also with predictions from design codes employing semi-empirical techniques.

LIST OF ILLUSTRATIONS

<u>Figure</u>		<u>Page</u>
1	Model Geometry (SOC).....	17
2	Expanded View of the Grid Near the SOC Projectile.....	18
3	Expanded View of the Grid in the Base Region.....	19
4	Variation of Pressure Drag Coefficient with Mach Number, $\alpha = 0$, SOC.....	20
5	Variation of Viscous Drag Coefficient with Mach Number, $\alpha = 0$, SOC.....	21
6	Variation of Base Drag Coefficient with Mach Number, $\alpha = 0$, SOC.....	22
7	Base Drag vs Mach Number at Transonic Speeds, $\alpha = 0$	23
8	Variation of Total Drag Coefficient with Mach Number, $\alpha = 0$, SOC.....	24
9	Model Geometry (SOCBT).....	25
10	Expanded View of the Grid for the SOCBT Projectile.....	26
11	Expanded View of the Grid in the Base Region.....	27
12	Variation of Pressure Drag Coefficient with Mach Number, $\alpha = 0$, SOCBT, $M = 0.8$ to 3.0	28
13	Variation of Pressure Drag Coefficient with Mach Number, $\alpha = 0$, SOCBT, $M = 0.9$ to 1.2	29
14	Variation of Viscous Drag Coefficient with Mach Number, $\alpha = 0$, SOCBT.....	30
15	Variation of Base Drag Coefficient with Mach Number, $\alpha = 0$, SOCBT, $M = 0.8$ to 3.0	31
16	Variation of Base Drag Coefficient with Mach Number, $\alpha = 0$, SOCBT, $M = 0.9$ to 1.2	32
17	Base Drag Comparison for SOC and SOCBT, $\alpha = 0$	33
18	Variation of Total Drag Coefficient with Mach Number, $\alpha = 0$, SOCBT.....	34
19	M549 Projectile.....	35
20	Computational Model.....	36

LIST OF ILLUSTRATIONS (Continued)

<u>Figure</u>		<u>Page</u>
21	Physical Grid for M549 Projectile.....	37
22	Velocity Vectors, $M_\infty = .9$, $\alpha = 0$, M549.....	38
23	Pressure Drag Coefficient vs Mach Number, $\alpha = 0$, M549.....	39
24	Viscous Drag Coefficient vs Mach Number, $\alpha = 0$, M549.....	40
25	Base Drag Coefficient vs Mach Number, $\alpha = 0$, M549.....	41
26	Total Drag Coefficient vs Mach Number, $\alpha = 0$, M549.....	42

I. INTRODUCTION

One of the most important aerodynamic performance characteristics for shell is the total drag. The total drag for projectiles can be divided into three components: (i) pressure drag (excluding the base), (ii) viscous (skin friction) drag, and (iii) base drag. The base drag is a major contributor to the total drag, particularly at transonic speeds. Thus, the determination of base pressure is essential in predicting the total drag for projectiles. The breakdown of the total drag into various components is important in the preliminary design stage of shell. This information can aid the designer to find potential areas for drag reduction and achieve a desired increase in range and/or terminal velocity of projectiles.

Design codes are available that can predict the individual drag components and thus, the total aerodynamic drag. Typically, the total drag predicted by these design codes agrees well with the total drag measured from flight tests. But, how well do these codes predict the individual drag components for a projectile? It is difficult to measure the individual drag components experimentally (especially the base drag and skin friction drag) and verify the accuracy of these predictions. Recently developed Navier-Stokes computational procedures are capable of predicting all the individual drag components for projectiles and can be used to determine how well the design codes predict the individual drag components. This report describes such a Navier-Stokes computational study to predict the individual drag components of projectiles and determine the accuracy of the predictions from available design codes.

II. COMPUTATIONAL TECHNIQUE

The Azimuthal Invariant (or Generalized Axisymmetric) thin-layer Navier-Stokes equations for general spatial coordinates ξ , n , ζ can be written as¹

$$\partial_{\tau} \hat{q} + \partial_{\xi} \hat{E} + \partial_{\zeta} \hat{G} + \hat{H} = \text{Re}^{-1} \partial_{\zeta} \hat{S} \quad (1)$$

where $\xi = \xi(x,y,z,t)$ is the longitudinal coordinate
 $n = n(y,z,t)$ is the circumferential coordinate
 $\zeta = \zeta(x,y,z,t)$ is the near normal coordinate
 $\tau = t$ is the time

and

-
1. C.J. Nietubicz, T.H. Pulliam, and J.L. Steger, "Numerical Solution of the Azimuthal-Invariant Navier-Stokes Equations," US Army Ballistic Research Laboratory, Aberdeen Proving Ground, Maryland, ARBRL-TR-02227, March 1980. (AD A085718) (Also see AIAA Journal, Vol. 18, No. 12, December 1980, pp. 1411-1412)

$$q = J^{-1} \begin{bmatrix} \rho \\ \rho u \\ \rho v \\ \rho w \\ e \end{bmatrix}, \quad \hat{E} = J^{-1} \begin{bmatrix} \rho U \\ \rho u U + \xi_x p \\ \rho v U + \xi_y p \\ \rho w U + \xi_z p \\ (e+p)U - \xi_t p \end{bmatrix}, \quad \hat{G} = J^{-1} \begin{bmatrix} \rho W \\ \rho u W + \zeta_x p \\ \rho v W + \zeta_y p \\ \rho w W + \zeta_z p \\ (e+p)W - \zeta_t p \end{bmatrix}$$

$$\hat{H} = J^{-1} \begin{bmatrix} 0 \\ 0 \\ \rho V [R_\xi (U - \zeta_t) + R_\zeta (W - \zeta_t)] \\ -\rho V R (V - \eta_t) - p/R \\ 0 \end{bmatrix}$$

$$\hat{S} = \begin{bmatrix} 0 \\ \mu(\zeta_x^2 + \zeta_y^2 + \zeta_z^2)u_\zeta + (\mu/3)(\zeta_x u_\zeta + \zeta_y v_\zeta + \zeta_z w_\zeta)\zeta_x \\ \mu(\zeta_x^2 + \zeta_y^2 + \zeta_z^2)v_\zeta + (\mu/3)(\zeta_x u_\zeta + \zeta_y v_\zeta + \zeta_z w_\zeta)\zeta_y \\ \mu(\zeta_x^2 + \zeta_y^2 + \zeta_z^2)w_\zeta + (\mu/3)(\zeta_x u_\zeta + \zeta_y v_\zeta + \zeta_z w_\zeta)\zeta_z \\ \{(\zeta_x^2 + \zeta_y^2 + \zeta_z^2)[(\mu/2)(u^2 + v^2 + w^2)_\zeta + \kappa p r^{-1}(\gamma - 1)^{-1}(a^2)_z] \\ + (\mu/3)(\zeta_x u + \zeta_y v + \zeta_z w)(\zeta_x u_\zeta + \zeta_y v_\zeta + \zeta_z w_\zeta)\} \end{bmatrix}$$

The velocities

$$U = \xi_t + \xi_x u + \xi_y v + \xi_z w$$

$$V = \eta_t + \eta_x u + \eta_y v + \eta_z w \quad (2)$$

$$W = \zeta_t + \zeta_x u + \zeta_y v + \zeta_z w$$

represent the contravariant velocity components.

The Cartesian velocity components (u, v, w) are nondimensionalized with respect to a_∞ (free stream speed of sound). The density (ρ) is referenced

to ρ_∞ and total energy (e) to $\rho_\infty a_\infty^2$. The local pressure is determined using the equation of state,

$$P = (\gamma - 1)[e - 0.5\rho(u^2 + v^2 + w^2)] \quad (3)$$

where γ is the ratio of specific heats.

In Equation (1), axisymmetric flow assumptions have been made which result in the source term, \hat{H} . The details of how this is obtained can be found in Reference 1 and are not discussed here. Equation (1) contains only two spatial derivatives. However, it retains all three momentum equations and allows a degree of generality over the standard axisymmetric equations. In particular, the circumferential velocity is not assumed to be zero, thus allowing computations for spinning projectiles to be accomplished.

The numerical algorithm used is the Beam-Warming fully implicit, approximately factored finite difference scheme. The algorithm can be first or second order accurate in time and second or fourth order accurate in space. Since the interest is only in the steady-state solution, Equation (1) is solved in a time asymptotic fashion and first order accurate time differencing is used. The spatial accuracy is fourth order. Details of the algorithm are included in References 2-4.

For the computation of turbulent flows, a turbulence model must be supplied. In the present calculations, the two layer algebraic eddy viscosity model developed by Baldwin and Lomax⁵ is used. In their two-layer model, the inner region follows the Prandtl-Van Driest formulation. Their outer formulation can be used in wakes as well as in attached and separated boundary layers. In both the inner and outer formulations, the distribution of vorticity is used to determine length scales, thereby avoiding the necessity of finding the outer edge of the boundary layer (or wake). The magnitude of the local vorticity for the axisymmetric formulation is given by:

-
2. J.L. Steger, "Implicit Finite Difference Simulation of Flow About Arbitrary Geometries with Application to Airfoils," AIAA Journal, Vol. 16, No. 7, July 1978, pp. 679-686.
 3. T.H. Pulliam and J.L. Steger, "On Implicit Finite-Difference Simulations of Three-Dimensional Flow," AIAA Journal, Vol. 18, No. 2, February 1980, pp. 159-167.
 4. R. Beam and R.F. Warming, "An Implicit Factored Scheme for the Compressible Navier-Stokes Equations," AIAA Journal, Vol. 15, No. 4, April 1978, pp. 393-402.
 5. B.S. Baldwin and H. Lomax, "Thin-Layer Approximation and Algebraic Model for Separated Turbulent Flows," AIAA Paper No. 78-257, 1978.

$$|\omega| = \sqrt{\left(\frac{\partial u}{\partial x}\right)^2 + \left(\frac{\partial v}{\partial z} - \frac{\partial w}{\partial y}\right)^2 + \left(\frac{\partial w}{\partial x} - \frac{\partial u}{\partial z}\right)^2} . \quad (4)$$

In determining the outer layer length scale a function⁵

$$F(y) = y|\omega| [1 - \exp(-y^+/A^+)] \quad (5)$$

was used where y^+ and A^+ are boundary layer parameters.

The thin-layer Navier-Stokes computational technique described above has been used in conjunction with a unique flow field segmentation procedure^{6,7} which allows the entire flow field over a projectile including the base region flow to be computed. An important advantage of this segmentation procedure lies in the preservation of the sharp corner at the base; in other words, no approximation or rounding of the actual sharp corner at the base is made. The details of this procedure can be found in References 6 and 7. Since the entire flow field over the projectile is calculated, all the individual drag components can be computed and thus, the total aerodynamic drag can be determined.

III. DESIGN CODES

A. NSWCAP

The NSWCAP code^{8,9} is a semi-empirical/analytical technique which provides fast predictions of static and dynamic coefficients of shell at transonic and low to moderate supersonic velocities. This code is relatively simple to use and is formulated to be a 'design tool'.

-
6. J. Sahu, C.J. Nietubicz, and J.L. Steger, "Numerical Computation of Base Flow for a Projectile at Transonic Speeds," US Army Ballistic Research Laboratory, Aberdeen Proving Ground, Maryland, ARBRL-TR-02495, June 1983. (AD A130293) (Also see AIAA Paper No. 82-1358, August 1982)
 7. J. Sahu, C.J. Nietubica, and J.L. Steger, "Navier-Stokes Computations of Projectile Base Flow with and without Base Injection," US Army Ballistic Research Laboratory, Aberdeen Proving Ground, Maryland, ARBRL-TR-02532, November 1983. (AD A135738) (Also see AIAA Journal, Vol. 23, No. 9, September 1985, pp. 1348-1355)
 8. F.G. Moore and R.C. Swanson, "Aerodynamics of Tactical Weapons to Mach Number 3 and Angle-of-Attack 15°, Part I - Theory and Application," NSWC/DL TR-3584, February 1977.
 9. F.G. Moore and R.C. Swanson, "Aerodynamics of Tactical Weapons to Mach Number 3 and Angle-of-Attack 15°, Part II - Computer Program and Usage," NSWC/DL TR 3600, March 1977.

The total drag is obtained by a linear superposition of pressure drag, skin friction drag and base drag. This code also has the ability to estimate the drag due to a rotating band if it is present.

The pressure drag consists of contributions from the nose and the boattail. The nose drag is based on empirical as well as experimental data at transonic speeds. The boattail pressure drag is based upon a small disturbance potential solution. The estimation of nose drag and boattail drag at supersonic speeds is based on the Van Dyke second-order theory¹⁰.

The skin friction component of the total drag is computed using the model of Van Driest¹¹. The base drag prediction is empirical. It is assumed that the boattail is located after a relatively long afterbody so that the approaching external flow is at free stream conditions. The base drag is determined by the expression

$$C_{AB} = -C_{p_{BA}}(M_\infty)(R_B/R_{ref})^2$$

where $C_{p_{BA}}(M_\infty)$ is the base pressure coefficient for a long afterbody with no boattail. R_B is the base radius and R_{ref} is the reference body radius (usually the radius of the cylindrical section). $C_{p_{BA}}$ is based on the data for a long cylindrical afterbody and a fully turbulent boundary layer ahead of the base. The effect of base bleed or rocket exhaust can not be accounted for in this approach.

B. MCDRAG

This is another program¹² based on semi-empirical technique which provides a quick response and is very easy to use. This code is used for estimating the drag of a projectile in the Mach number range of 0.5 to 5.0. The total drag takes the form

$$C_{D_0} = C_{D_p} + C_{D_v} + C_{D_B}$$

-
10. M.J. Van Dykes, "The Similarity Rules for Second-Order Subsonic and Supersonic Flow," NACA Tech Note 3875, October 1956.
 11. E.R. Van Driest, "Turbulent Boundary Layers in Compressible Fluids," *Journal of the Aeronautical Sciences*, Vol. 18, No. 3, 1951, pp. 145-160.
 12. R.L. McCoy, "McDrag - A Computer Program for Estimating the Drag Coefficient of Projectiles," US Army Ballistic Research Laboratory, Aberdeen Proving Ground, Maryland, ARBRL-TR-02293, February 1981. (AD A098110)

where C_{D_0} = total drag coefficient at zero angle of attack

C_{D_p} = pressure drag or wave drag coefficient

C_{D_v} = viscous or skin friction drag coefficient

C_{D_B} = base drag coefficient.

The pressure drag consists of drag due to the projectile nose, boattail and the rotating band (if any). Prediction of the projectile nose drag is based on analytical theories at supersonic speeds while the transonic nose drag is based on correlations with experimental data. This is similar to the procedure used in the NSWCAP code. The effect of leading edge bluntness is accounted for in estimating the nose drag. As for the boattail drag, second order theory is used to correlate with experimental data to estimate this component of drag at supersonic speeds and a similar procedure is used at transonic speeds as well. The drag due to the rotating band is usually very small (of the order a few percent of the total drag) and is based on correlations with few experimental tests.

The skin friction drag coefficient, C_{D_v} , is given by,

$$C_{D_v} = \frac{4}{\pi} C_F S_W$$

where C_F = skin friction coefficient for a smooth flat plate

S_W = projectile wetted surface area (excluding the base)

C_F is estimated analytically depending on whether the boundary layer is laminar or turbulent on the nose. The flow over the afterbody is assumed to be turbulent always.

The base drag coefficient, C_{D_B} is estimated empirically. The approach taken here differs from the procedure used in the NSWCAP code. The pressure drag and skin friction drag are estimated as described previously. These contributions are then subtracted out from the measured total drag coefficients which are available from free flight data of various projectiles. An average base pressure is then inferred from the derived base drag coefficient. The estimate of base drag coefficient is obtained from the relation,

$$C_{D_B} = \frac{2d_B^2}{\gamma M_\infty^2} \left(1 - \frac{P_B}{P_\infty}\right)$$

where P_B/P_∞ = base pressure obtained from a least square fit of the data which includes Mach number and boattail effects

and d_B = diameter at the base.

IV. RESULTS

Computations of various drag components, and thus the total drag have been made for three projectiles: SOC; SOCBT; and the M549. For the Navier-Stokes computations, solutions were marched in time until the steady state results were achieved. Results are now presented for the three cases considered.

A. SOC Configuration

This projectile has a 3 caliber (1 caliber \equiv 1 reference body diameter) secant-ogive nose and a 3 caliber cylindrical afterbody as shown in Figure 1. One of the first steps before performing Navier-Stokes calculations is the determination of a computational grid. An expanded view of the grid near the projectile is shown in Figure 2. The grid consists of 114 points in the longitudinal direction (including 30 points in the base region) and 50 points in the normal direction. The grid points in the normal direction are stretched away from the surface exponentially. The clustering near the body surface is required to resolve the boundary layer. Additional grid clustering is used in the longitudinal direction near the nose-cylinder junction and the base where appreciable changes in the flow field variables are expected. Figure 3 shows an expanded view of the grid in the base region. Fifty grid points are used in the base region from the base corner down to the center line of symmetry. This is done to provide adequate grid resolution along the base of the projectile.

The individual drag components (pressure drag, viscous drag and base drag) are obtained from the computed solutions and their variations with Mach number are presented next. These results are compared with the predictions from the design codes. As shown in Figure 4, the pressure drag predicted by the Navier-Stokes code agrees well with the MCDRAG and NSWCAP predictions except at $M = 1.2$ where a small discrepancy is found. Comparison of viscous drag is shown in Figure 5. Here the viscous drag predicted by the Navier-Stokes code is in very good agreement with the MCDRAG prediction. The NSWCAP code underpredicts this drag by about 15% in the transonic speed regime. This contribution to the total drag is, however, small.

Figure 6 shows the variation of base drag as a function of Mach number. As expected, the base drag decreases as Mach number is increased from 1.2 to 3. For this range of speeds the Navier-Stokes code result agrees very well with the NSWCAP prediction. MCDRAG overpredicts these results by about 12%.

Comparison of the base drag is shown more clearly in Figure 7. The Navier-Stokes results are indicated by circles, experimental results¹³ by triangles, data base¹⁴ results by diamonds and MCDRAG results by squares. The results from the data base are based on correlation of base pressures obtained from a number of experiments and other analytical techniques. The increase in base drag with increase in Mach number in the transonic regime is predicted by all techniques. However, large scatter in the predictions of base drag exists. The Navier-Stokes result agrees well with the result from the data base except at $M = 1.1$ where it overpredicts the base drag by 12%. The MCDRAG prediction of base drag is consistently higher (up to 10%) than the data base result.

The total aerodynamic drag is obtained from the individual components and is plotted as a function of Mach number in Figure 8. The Navier-Stokes result compares very well with NSWCAP prediction at all speeds (transonic and supersonic). The MCDRAG prediction is in reasonable agreement with other results at higher Mach numbers ($M > 1$); however, discrepancy up to 20% is found at low Mach numbers ($0.9 < M < 1.0$). The total drag, as expected, increases as Mach number increases from 0.9 to 1.2 in the transonic speed regime.

B. SOCBT Configuration

The model geometry for this secant-ogive-cylinder-boattail (SOCBT) configuration is shown in Figure 9. It has a 3 caliber secant-ogive nose, a 2 caliber cylinder and a 1 caliber, 7° boattail. A computational grid was obtained for this configuration and an expanded view of the grid near the projectile is shown in Figure 10. This grid consists of 114 points in the streamwise direction and 50 points in the normal direction. Grid clustering in the streamwise direction has been used near the ogive-cylinder and cylinder-boattail junctions as well as the base. Figure 11 shows the expanded view of the grid in the base region and again shows the large number of grid points used in this region.

The drag components (pressure drag, viscous drag and base drag) for this shape are shown in Figures 12 through 18. Figure 12 shows the pressure drag comparison. At higher supersonic Mach numbers all predictions are in reasonable agreement. The pressure drag at transonic speeds is under predicted by both the design codes. As shown in Figure 13 the pressure drag

13. L.D. Kayser, "Base Pressure Measurements on a Projectile Shape at Mach Numbers for 0.91 to 1.20," US Army Ballistic Research Laboratory, Aberdeen Proving Ground, Maryland, ARBRL-MR-03363, April 1984. (AD A141341)

14. P.R. Payne and R.M. Hartley, "Afterbody Drag, Volume 1 - Drag of Conical and Circular Arc Afterbodies without Jet Flow," Final Report, DTNSRDC/ASED-80/10, Bethesda, Maryland, May 1980.

obtained from the Navier-Stokes results is compared with experiment¹⁵ and is in excellent agreement with experiment. The viscous drag is compared in Figure 14. The Navier-Stokes result is in good agreement with the MCDRAG prediction at all Mach numbers from .9 to 3.0. The NSWCAP code prediction is in reasonable agreement at supersonic Mach numbers and is underpredicted at all transonic Mach numbers. Comparison of the base drag is shown in Figure 15. As shown in this figure, the Navier-Stokes code prediction is in good agreement with the predictions from the design codes at higher Mach numbers ($M > 1.5$). Large discrepancies are seen between the predictions at transonic speeds. Both design codes MCDRAG and NSWCAP grossly overpredict the base drag in this speed regime. The Navier-Stokes result is compared with experiment¹³ and the MCDRAG result in Figure 16. Although there is a small discrepancy between the numerical result and the experimental data, the trend i.e., decrease and increase of base drag with Mach number seen experimentally is clearly observed in the computational results. MCDRAG, on the other hand, does not show the correct trend and grossly overpredicts the base drag except at $M = 1.2$. NSWCAP, predicts even higher base drag at transonic speeds and thus, is in worse agreement with the Navier-Stokes result and the experiment. The computational result and the experiment show a negative base drag (or thrust) at Mach numbers 0.94, 0.96 and 0.98 which is not predicted by the design codes.

Figure 17 shows the variation of base drag with Mach number for both SOC and SOCBT configurations. These are the computational results and the reduction in base drag due to the boattail is clearly seen. Figure 18 shows the total drag as a function of Mach number. The Navier-Stokes result is compared with the design code predictions. The agreement is good at all Mach numbers except between 1.1 and 1.2 where about 15-20% discrepancy is found between the design code predictions and the Navier-Stokes result.

C. M549 Projectile

The M549 is a modern, low drag, Army artillery shell. The geometry of this shell is shown in Figure 19. It has a 3 caliber ogive nose, an approximately 2 caliber cylindrical section, and a .59 caliber, $7\ 1/2^\circ$ boattail. Certain simplifications have been made on this shape. The flat nose was modeled as a hemisphere cap and the rotating band was eliminated. As a result, a modified configuration, shown in Figure 20, was obtained and used for the numerical computations.

An expanded view of the computational grid near the projectile is shown in Figure 21. This grid has 114 points in the streamwise direction and 40 points in the normal direction. Grid points are clustered near the surface and also in the base region where large changes in the flow variables are expected. Figure 22 shows the velocity vectors in the base region obtained from the Navier-Stokes calculations. The recirculatory base flow is clearly evident.

15. L.D. Kayser, "Surface Pressure Measurements on a Boattailed Projectile Shape at Transonic Speeds," US Army Ballistic Research Laboratory, Aberdeen Proving Ground, Maryland, ARBRL-MR-03181, March 1982. (AD A113520)

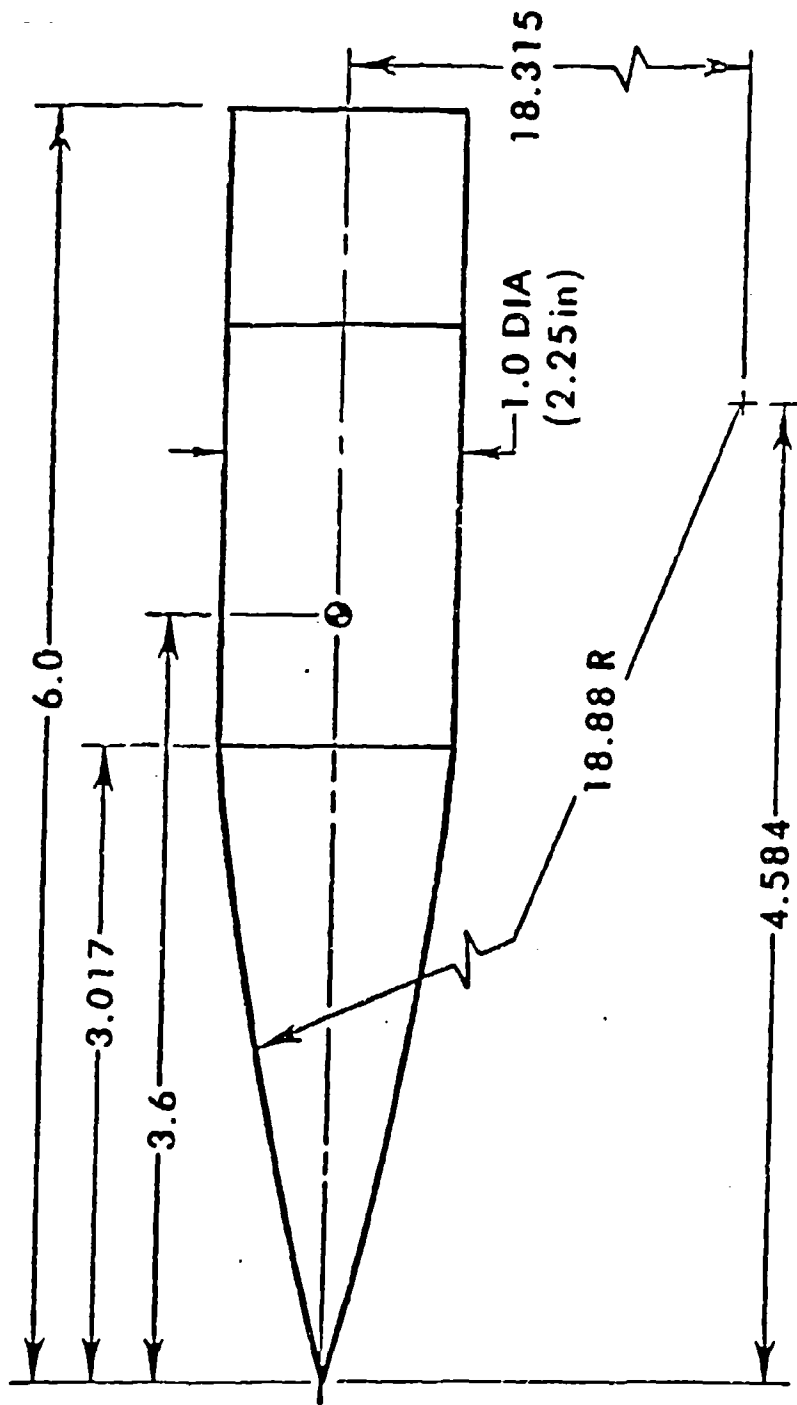
The individual drag components (pressure drag, viscous drag, base drag) and the total drag are shown in Figures 23, 24, 25 and 26, respectively. The drag components obtained from Navier-Stokes solutions are compared with the NSWCAP and MCDRAG predictions. The pressure drag predicted by the Navier-Stokes code, NSWCAP code and MCDRAG is in good agreement at low Mach numbers ($.9 < M < 1.0$). MCDRAG predicts slightly higher pressure drag at higher Mach numbers compared to the Navier-Stokes and NSWCAP predictions. The viscous drag predicted by all codes is in good agreement. As for the base drag, the Navier-Stokes result agrees very well with the NSWCAP prediction whereas MCDRAG underpredicts the base drag by as much as 20 to 25%. The total drag comparison is shown in Figure 26. Again, the Navier-Stokes result is compared with predictions from NSWCAP and MCDRAG codes. In addition, these predictions are compared with the LCWSL¹⁶ data base and are all in good agreement.

IV. CONCLUDING REMARKS

A thin-layer Navier-Stokes code has been used to compute the flow field over projectiles including the base region. Numerical computations have been made for three projectiles (SOC, SOCBT and M549) for various Mach numbers and $\alpha = 0$. The individual drag components (pressure drag, viscous drag, and base drag) and total drag were obtained from computed solutions. In addition, two design codes (NSWCAP and MCDRAG) that employ semi-empirical techniques were used to predict the drag for projectiles. Predictions from the Navier-Stokes code and the design codes were compared with experiment and/or data base results where available.

The viscous drag predicted by the design codes is generally in good agreement with the prediction from the Navier-Stokes code. However, significant discrepancies in the prediction of pressure drag and base drag are found. When pressure drag is underpredicted, the base drag is overpredicted and vice versa. Thus, when the individual drag components are added up to obtain the total drag, the discrepancy is usually small and reasonably good agreement is found between the predictions of total drag from the Navier-Stokes code and the design codes.

16. A. Loeb, "Private Communication," Large Caliber Weapons Systems Laboratory, ARDC, AMCCOM, Dover, New Jersey.



ALL DIMENSIONS IN CALIBERS

Figure 1. Model Geometry (SOC)

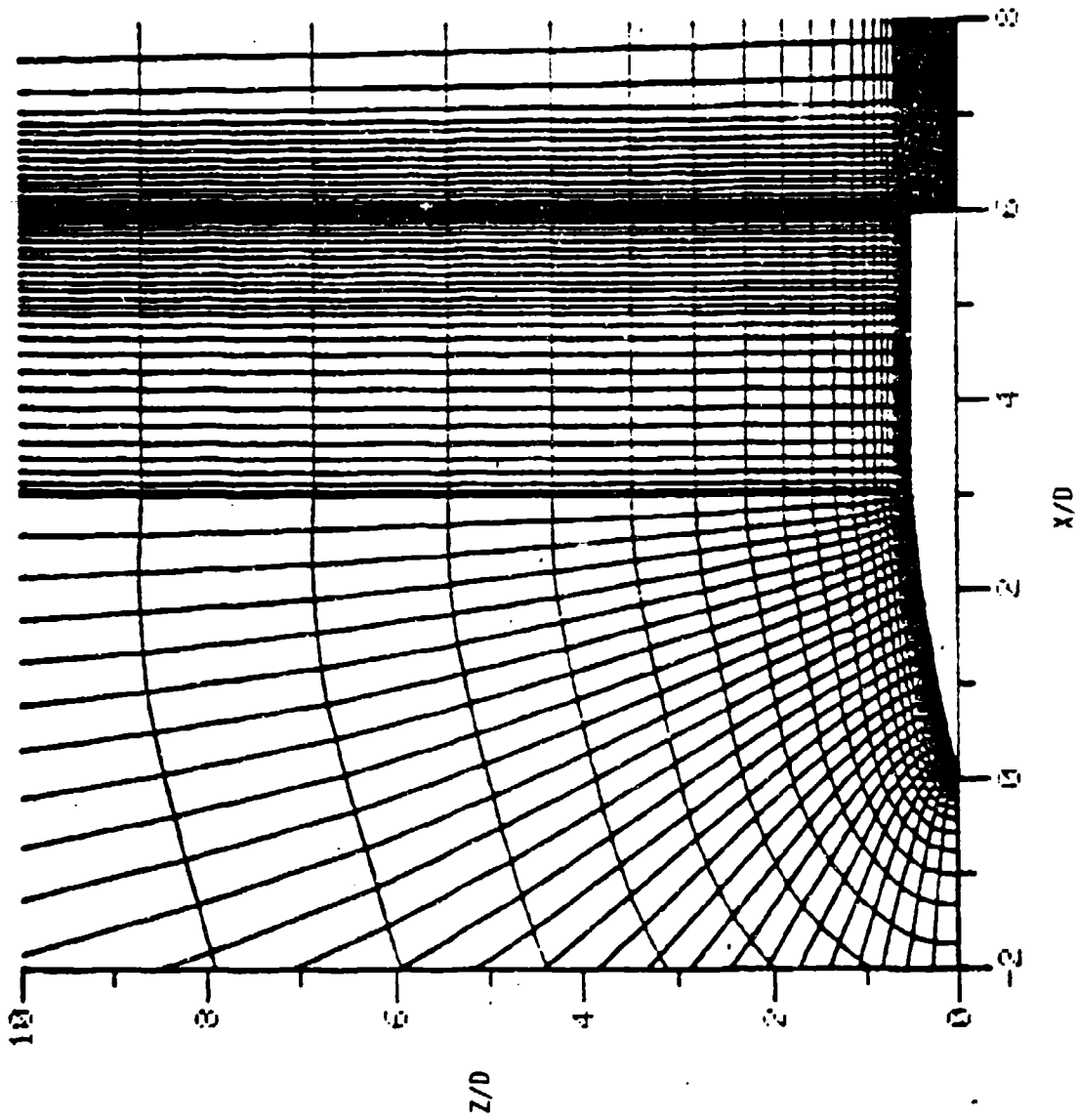


Figure 2. Expanded View of the Grid Near the SOC Projectile

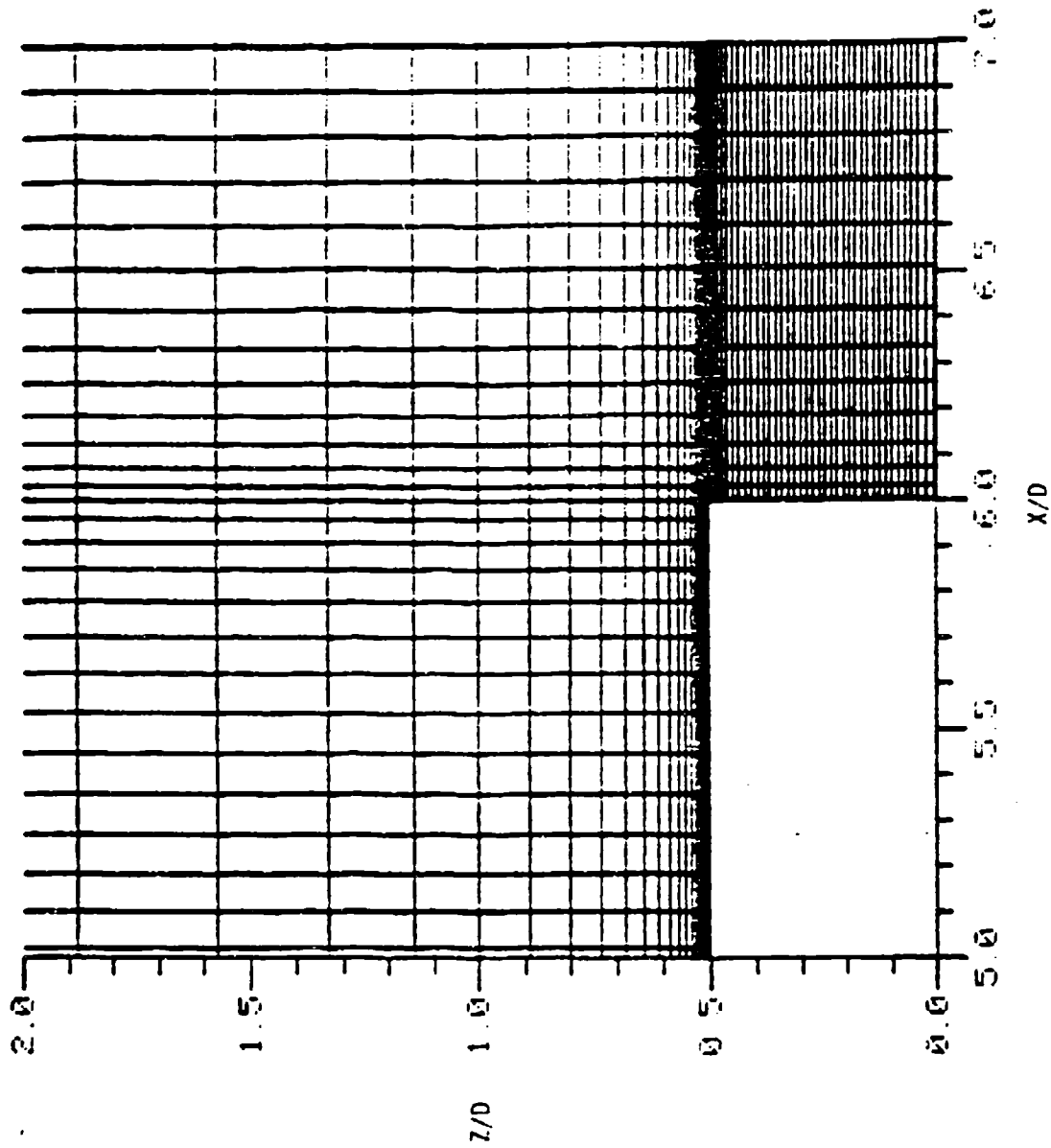


Figure 3. Expanded View of the Grid in the Base Region

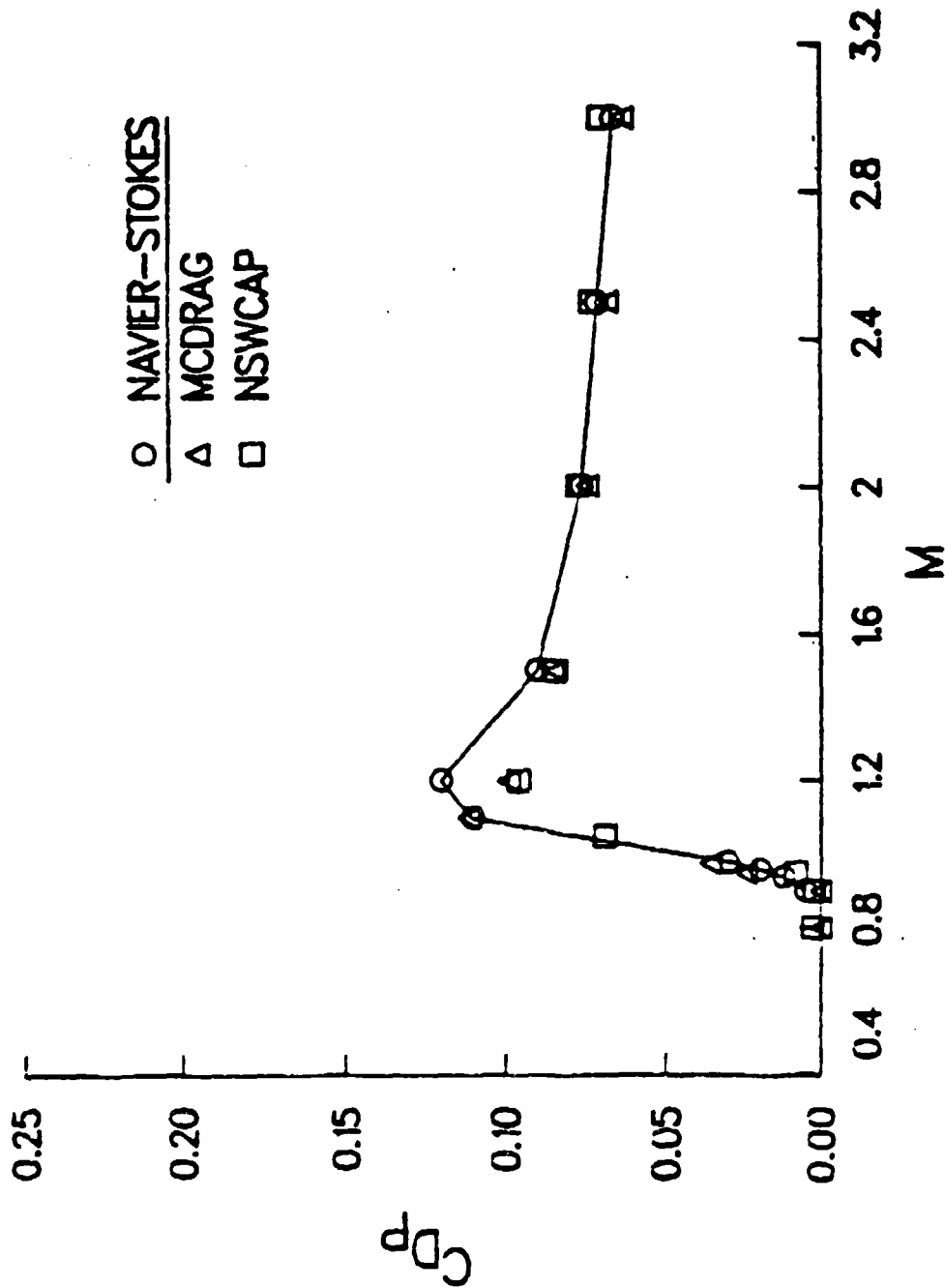


Figure 4. Variation of Pressure Drag Coefficient with Mach Number, $\alpha = 0$, SOC

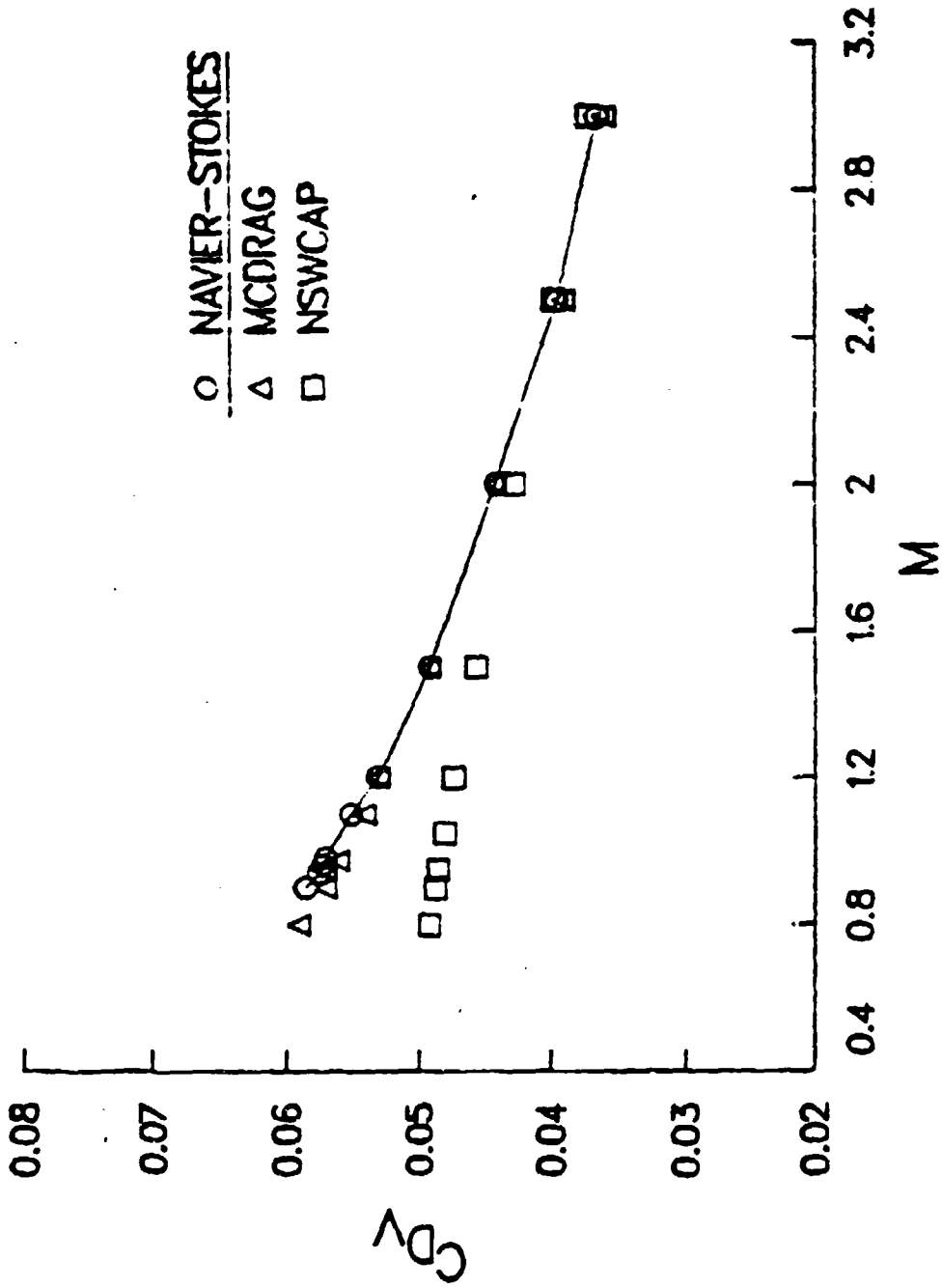


Figure 5. Variation of Viscous Drag Coefficient with Mach Number, $\alpha = 0$, SOC

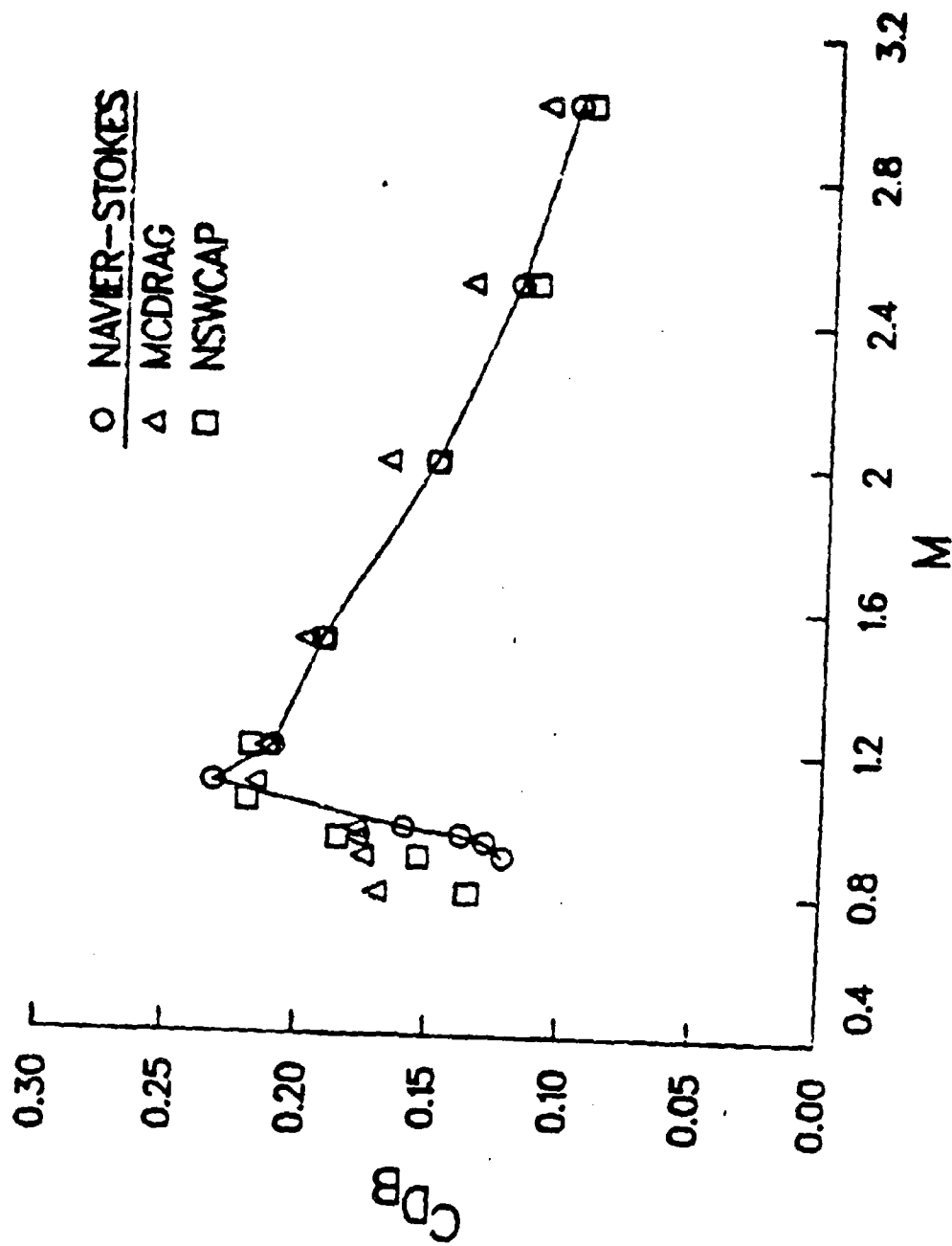


Figure 6. Variation of Base Drag Coefficient with Mach Number, $\alpha = 0$, SOC

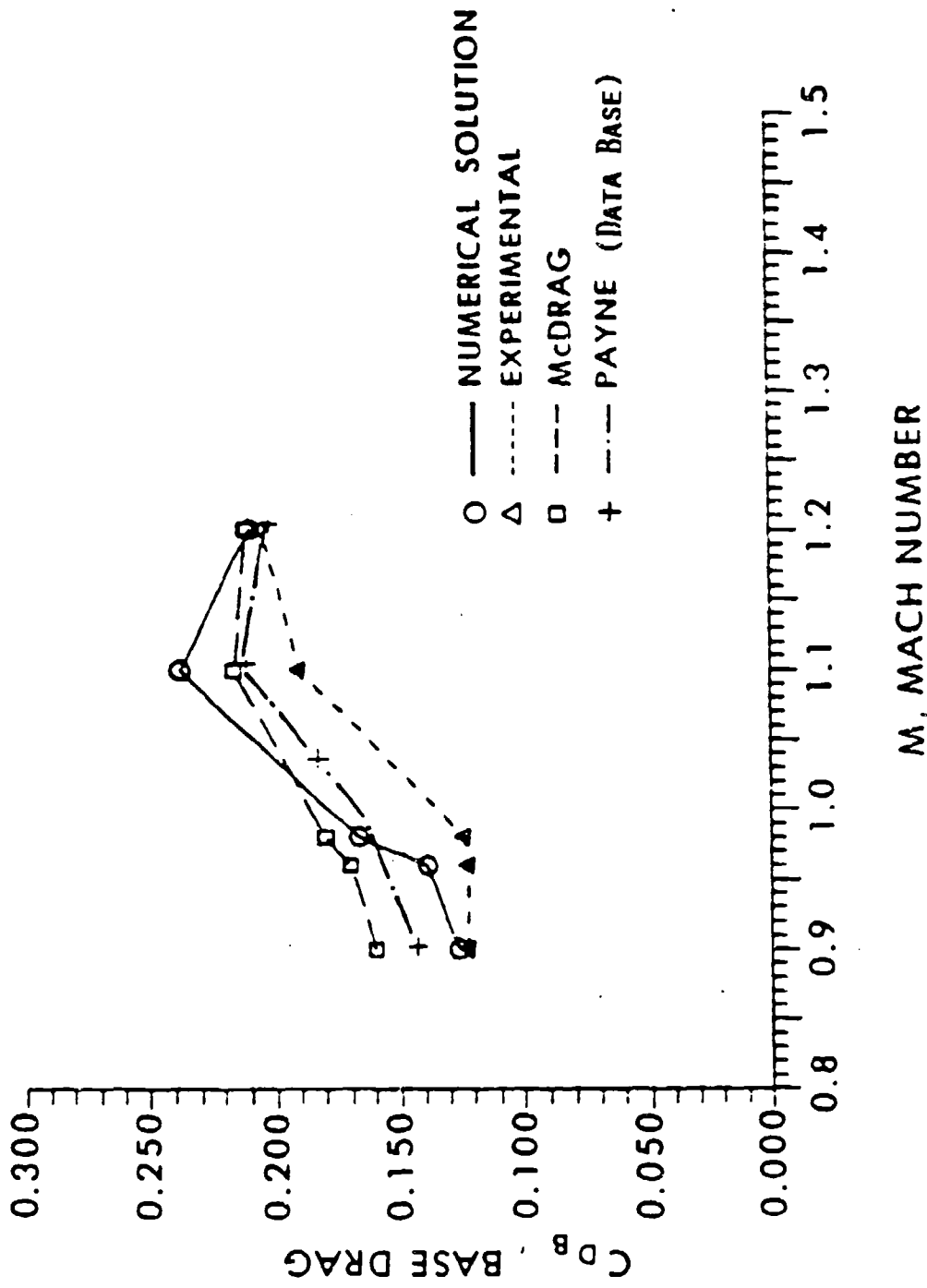


Figure 7. Base Drag vs Mach Number at Transonic Speeds, $\alpha = 0$

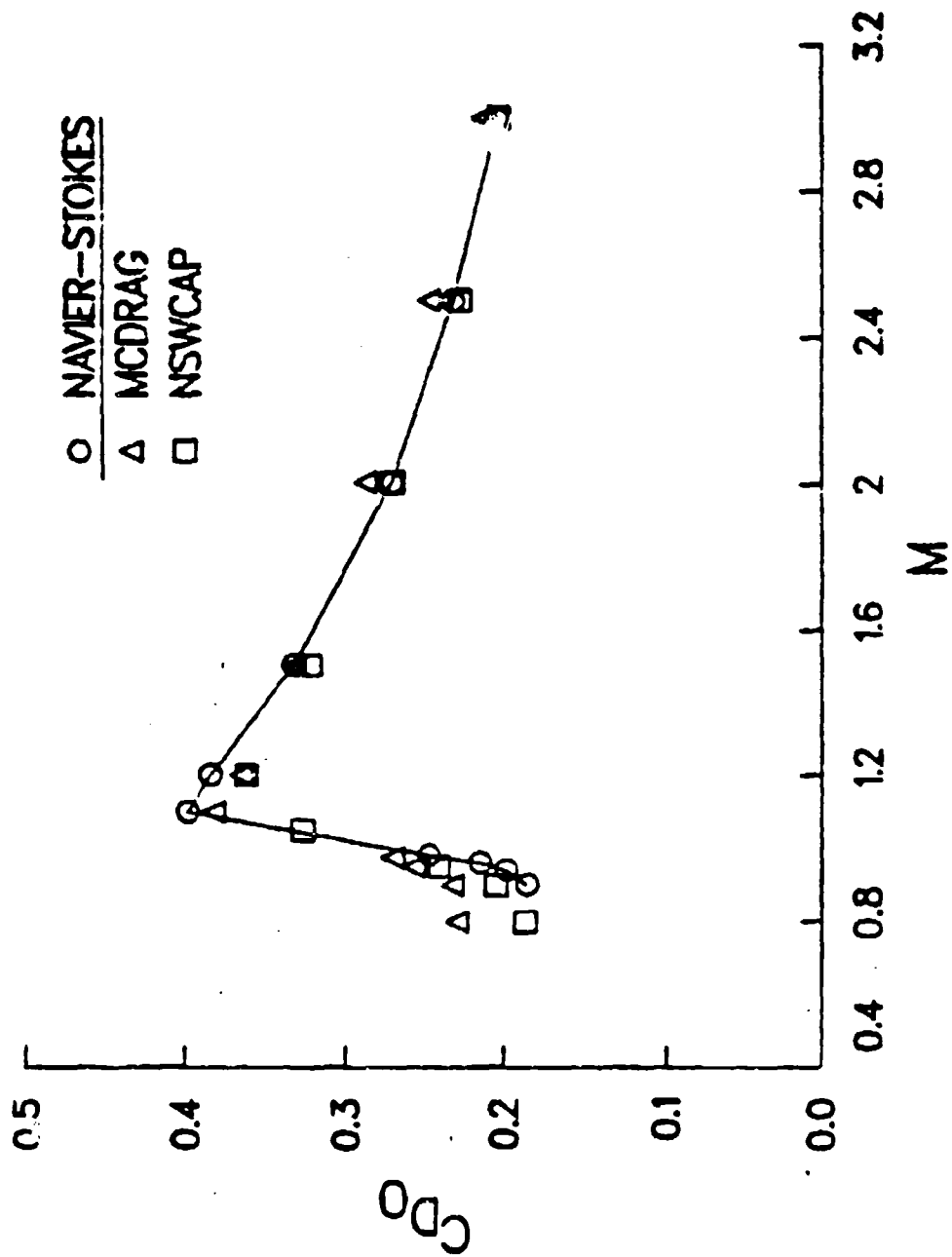
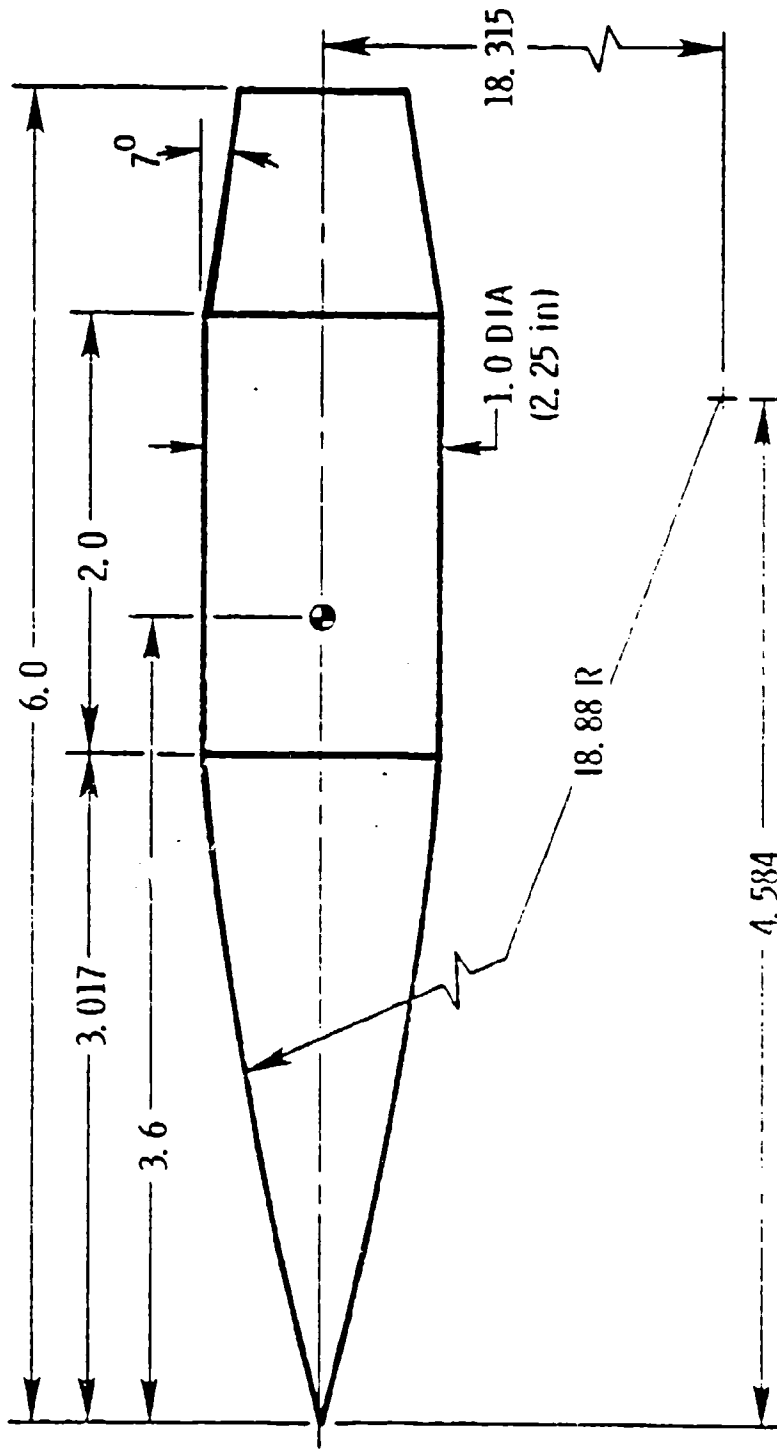


Figure 8. Variation of Total Drag Coefficient with Mach Number, $\alpha = 0$, SOC



ALL DIMENSIONS IN CALIBERS

Figure 9. Model Geometry (SOCBT)

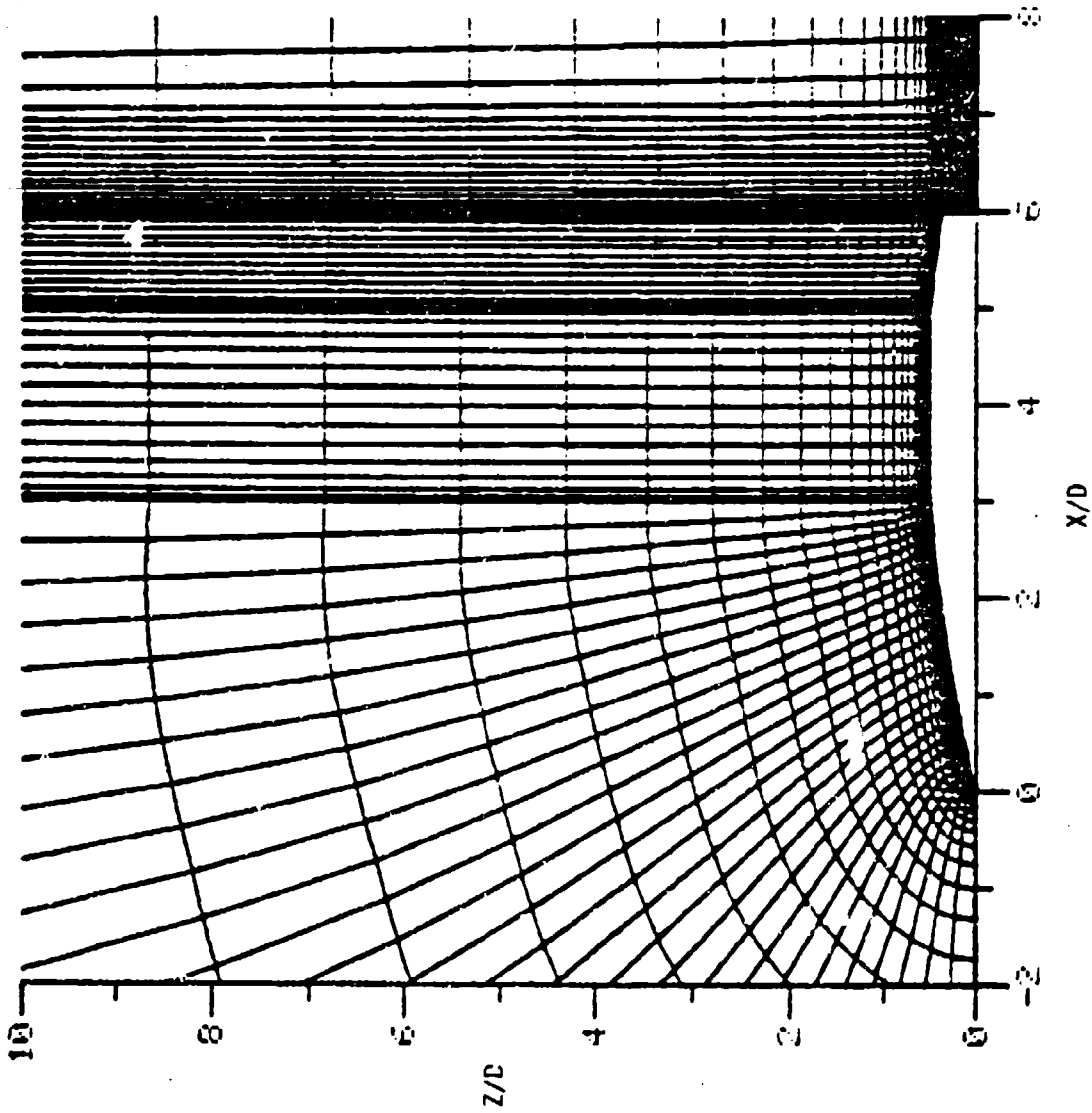


Figure 10. Expanded View of the Grid for the S0CBT Projectile

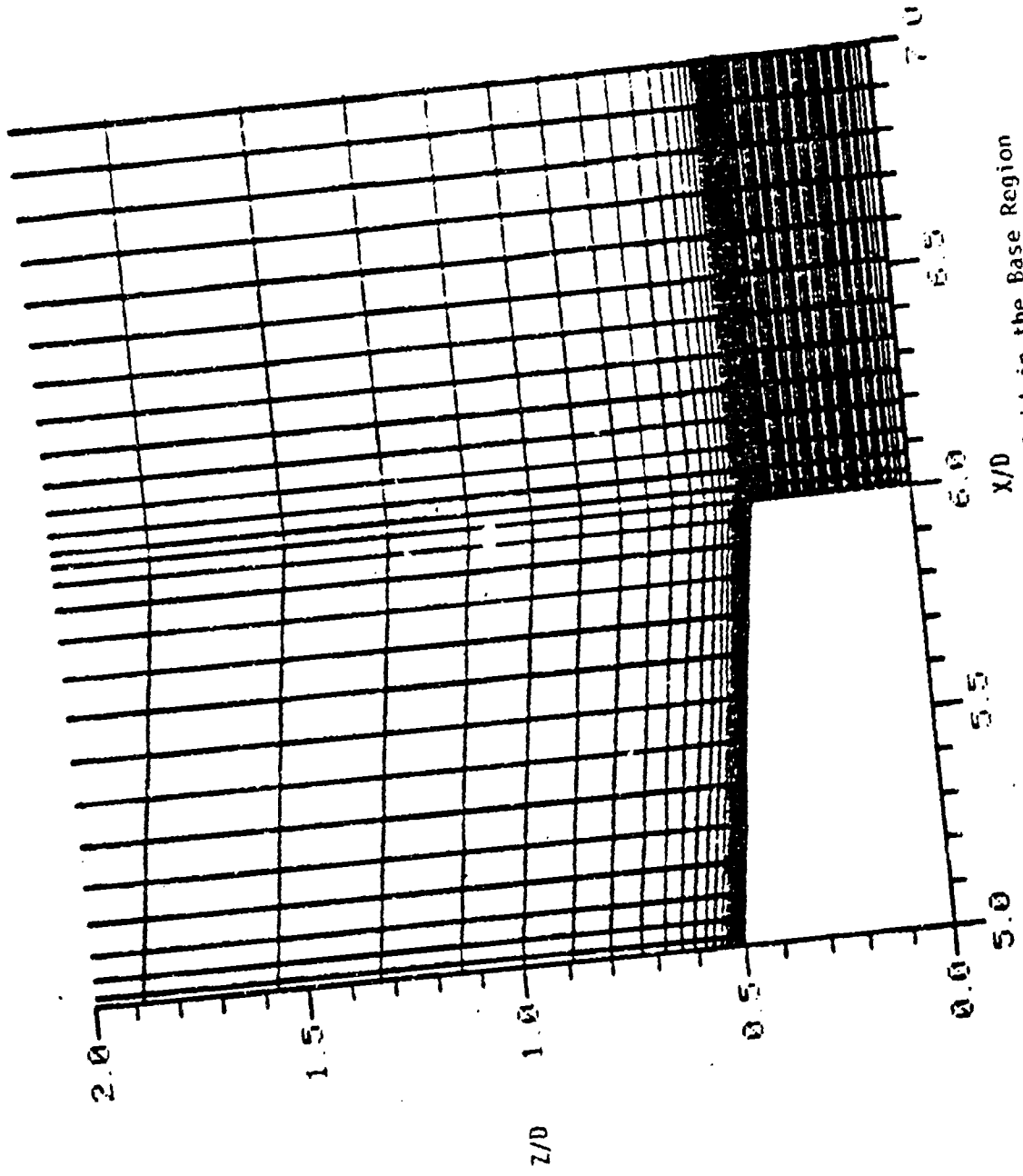


Figure 11. Expanded View of the Grid in the Base Region

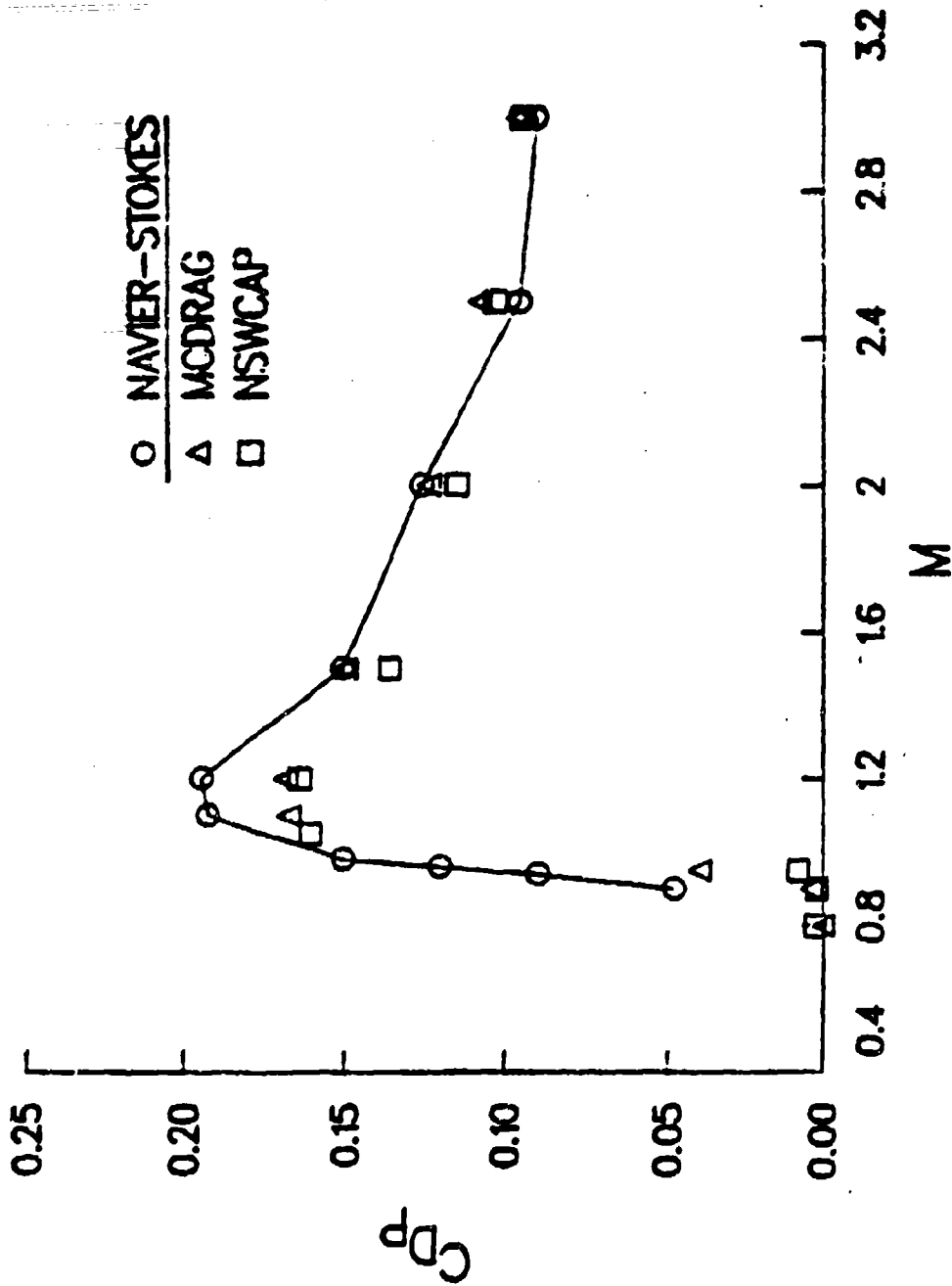


Figure 12. Variation of Pressure Drag Coefficient with Mach Number, $\alpha = 0$, SOCBT, $M = 0.8$ to 3.0

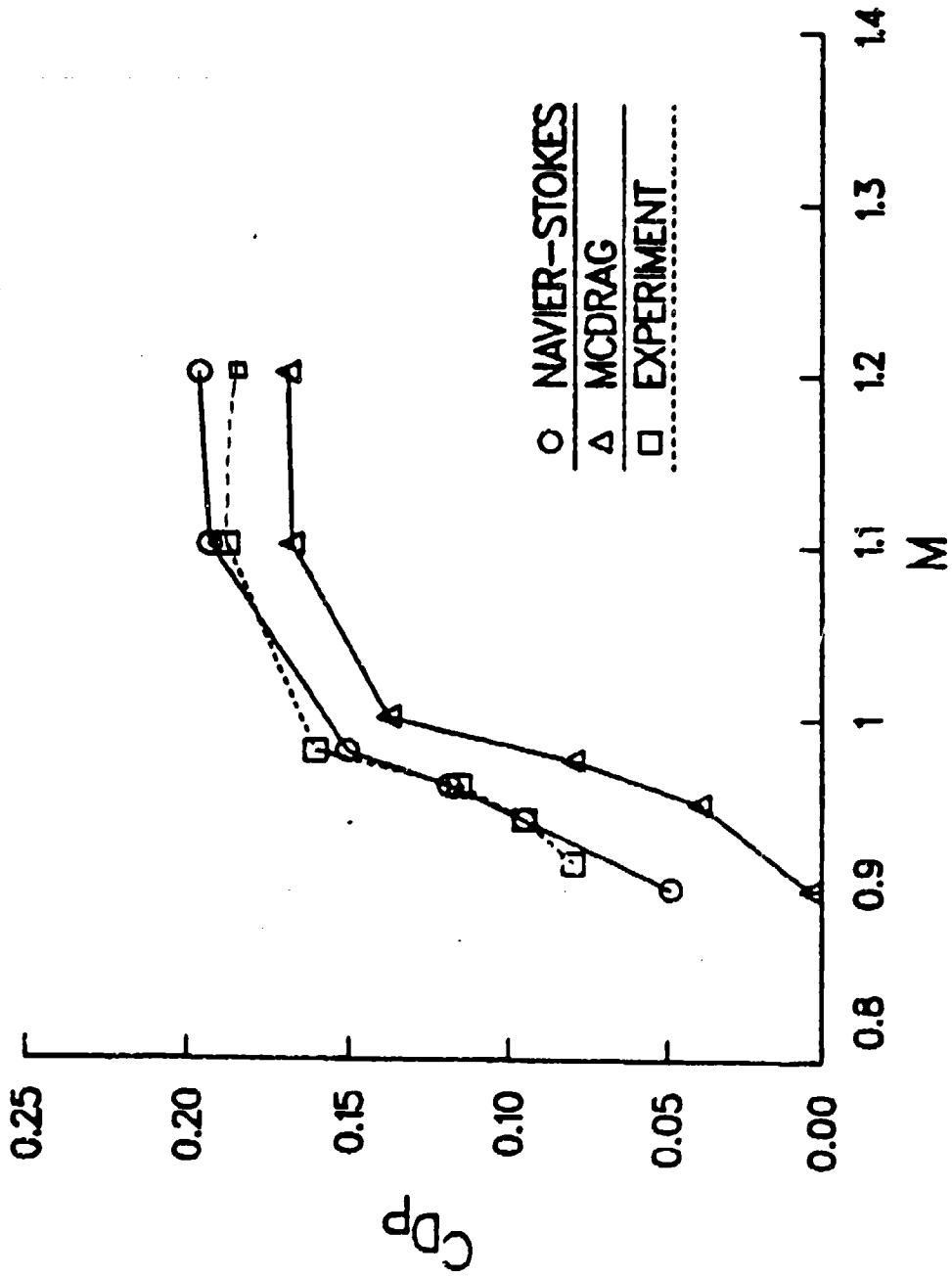


Figure 13. Variation of Pressure Drag Coefficient with Mach Number, $\alpha = 0$, SOCBT, $M = 0.9$ to 1.2

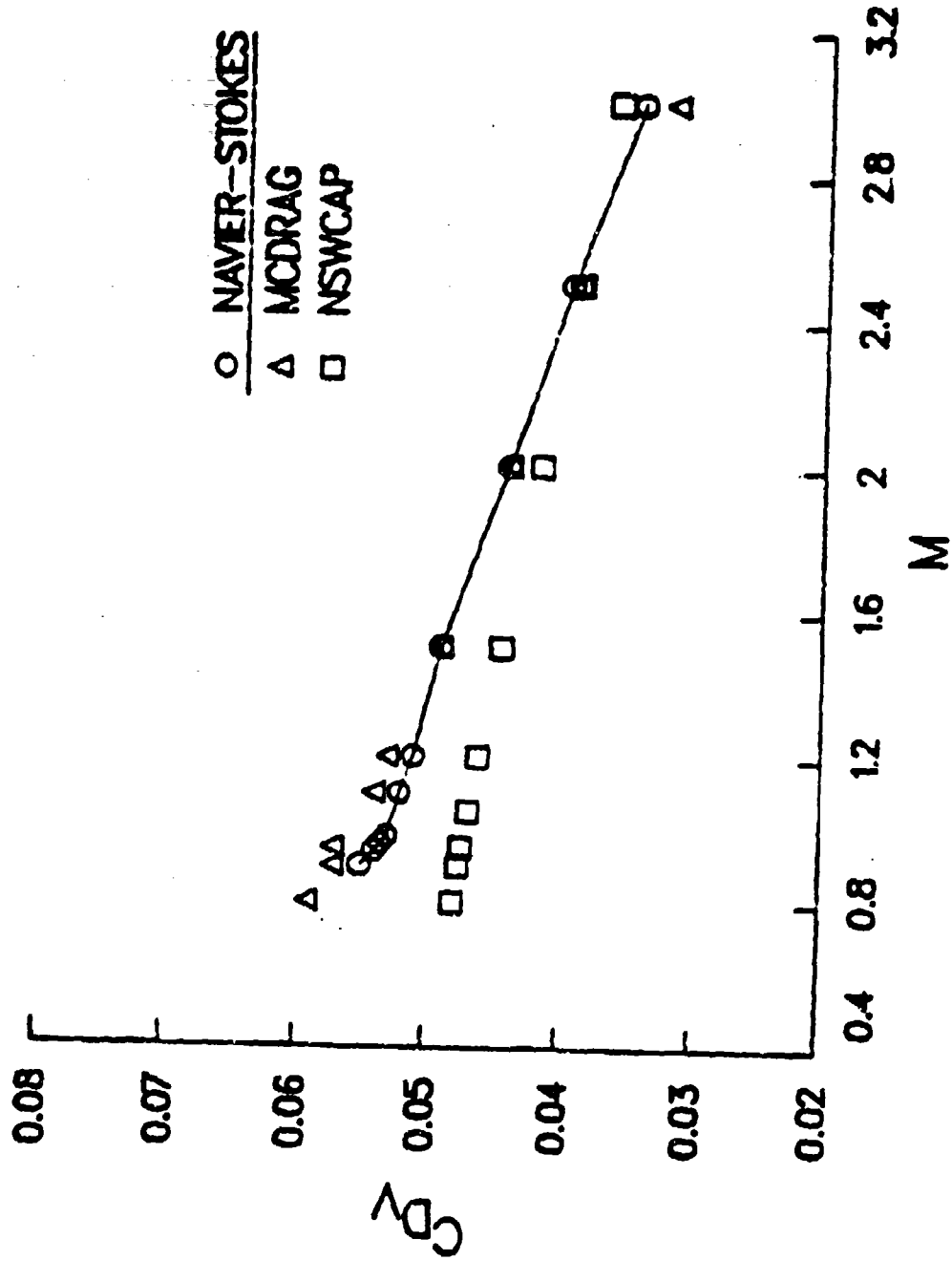


Figure 14. Variation of Viscous Drag Coefficient with Mach Number, $\alpha = 0$, SOCRT

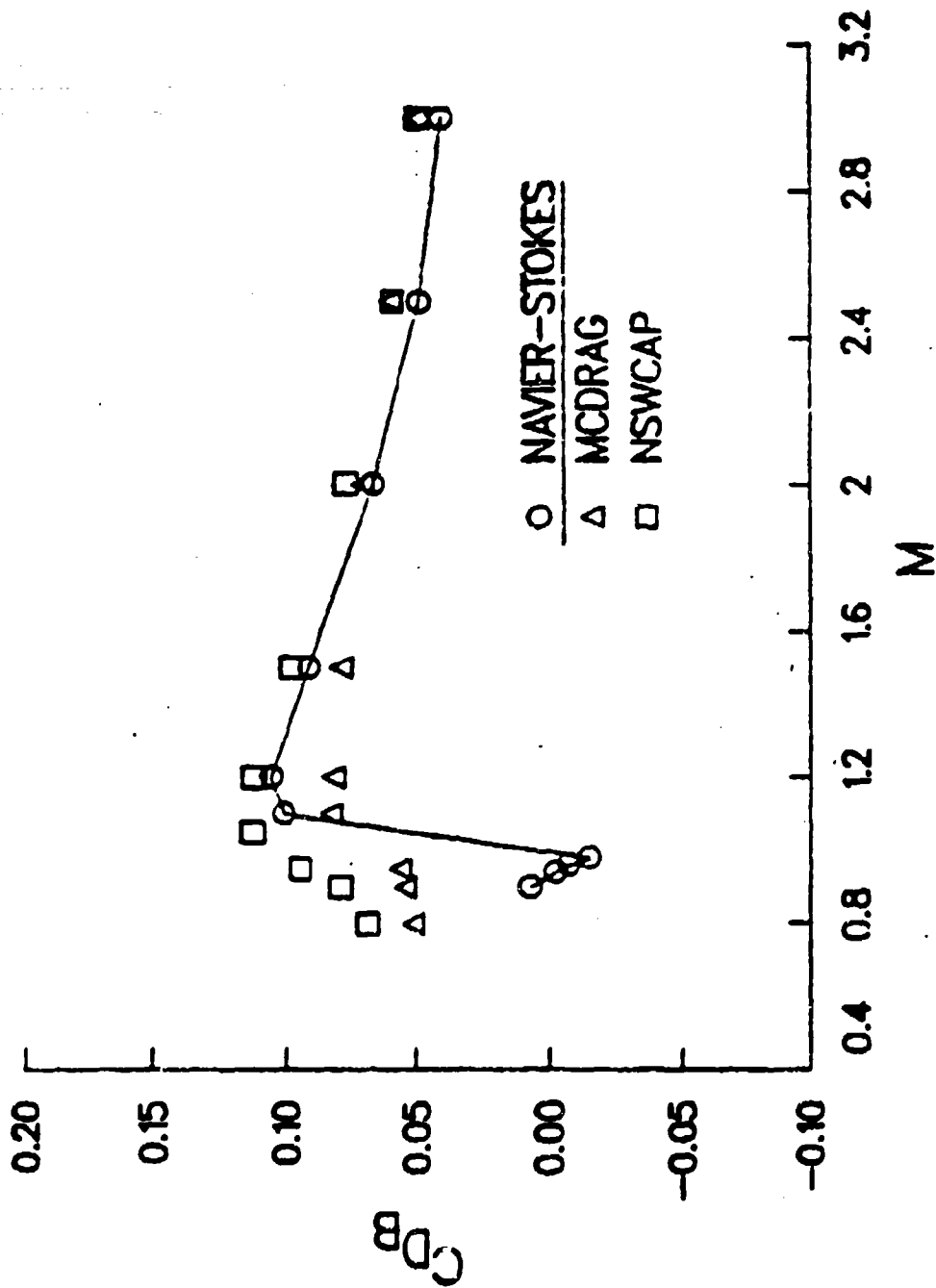


Figure 15. Variation of Base Drag Coefficient with Mach Number, $\alpha = 0$, SOCBT, $M = 0.8$ to 3.0

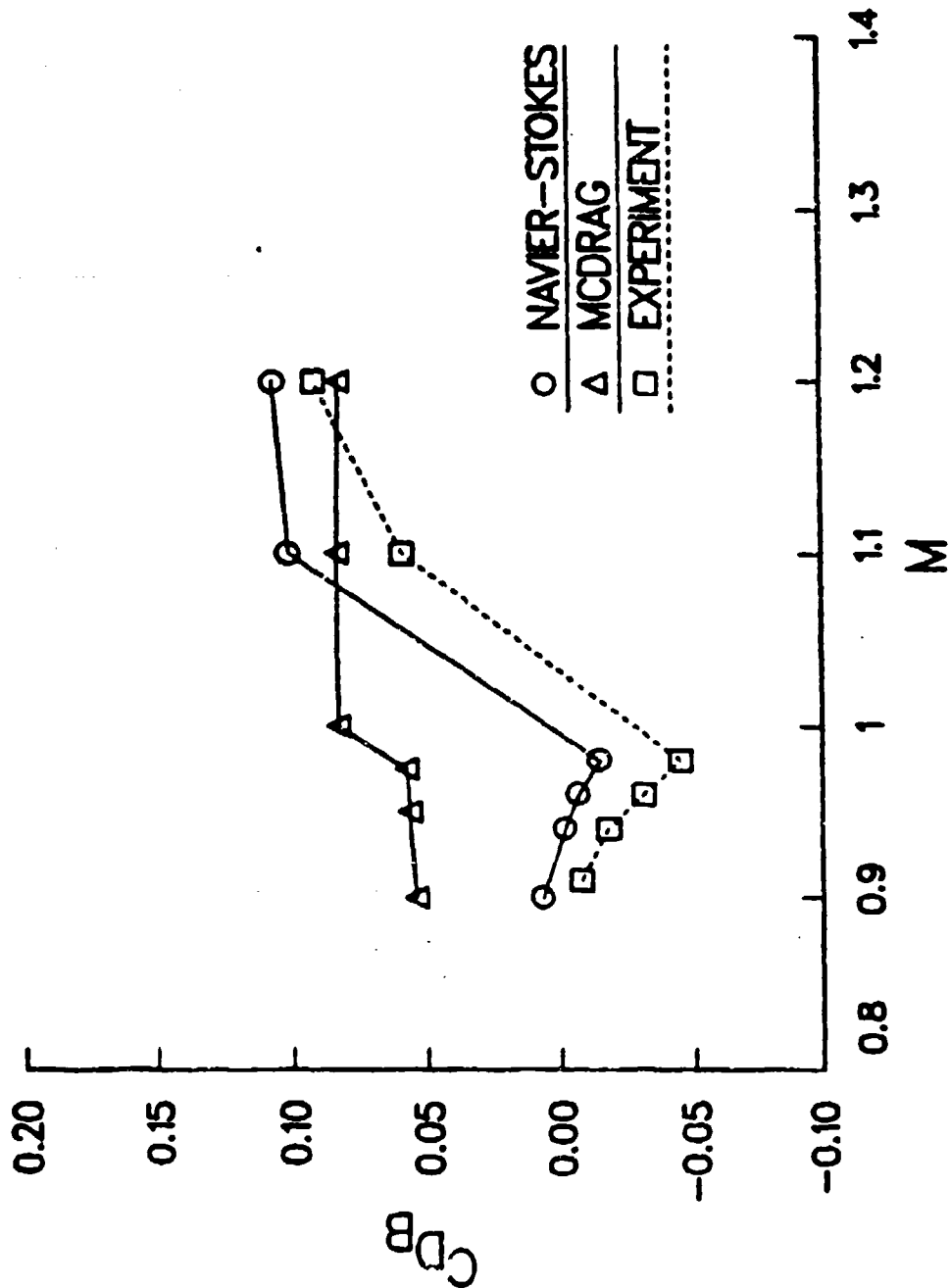


Figure 16. Variation of Base Drag Coefficient with Mach Number
 $\alpha = 0$, SOCBT, $M = 0.9$ to 1.2

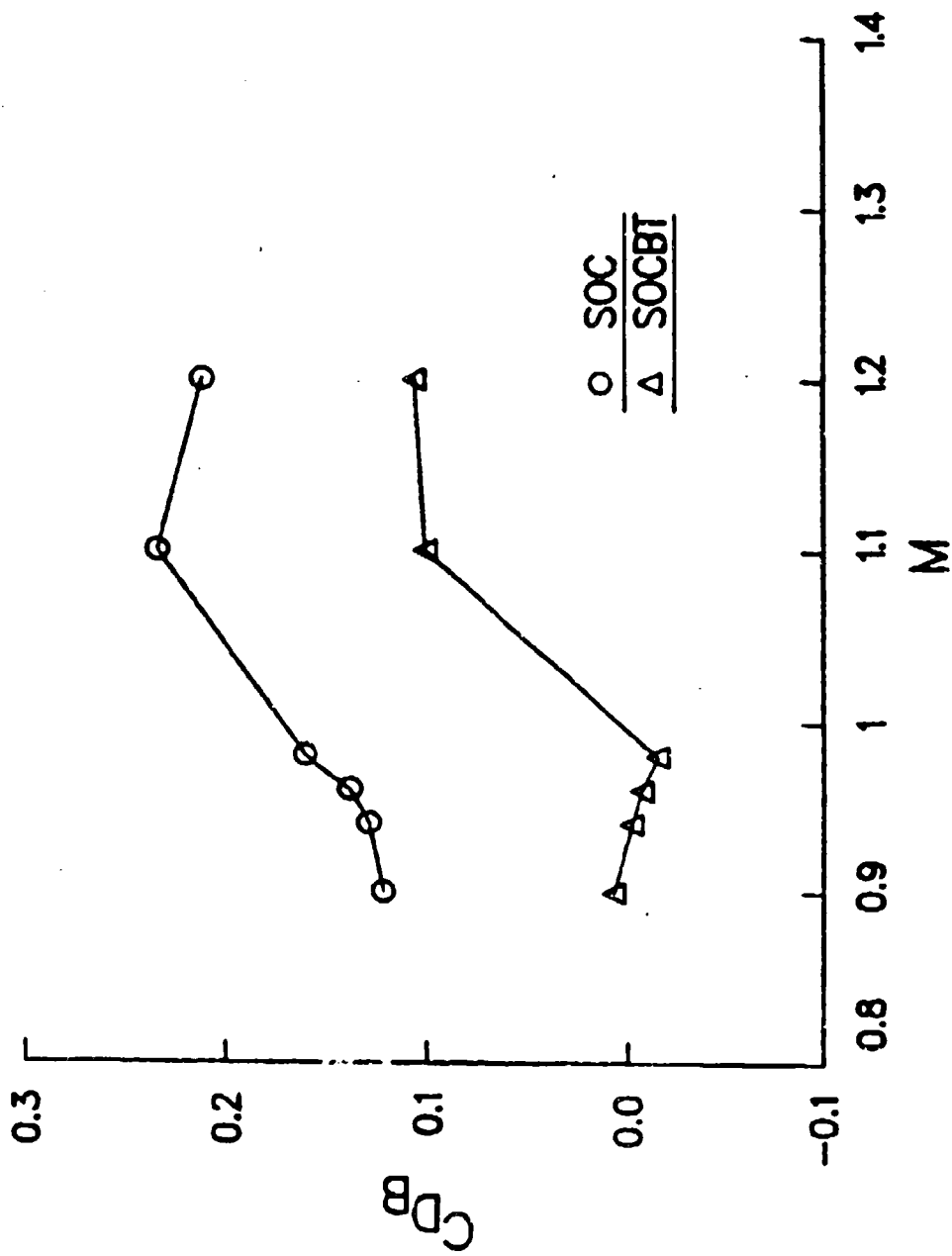


Figure 17. Base Drag Comparison for SOC and SOCBT, $\alpha = 0$

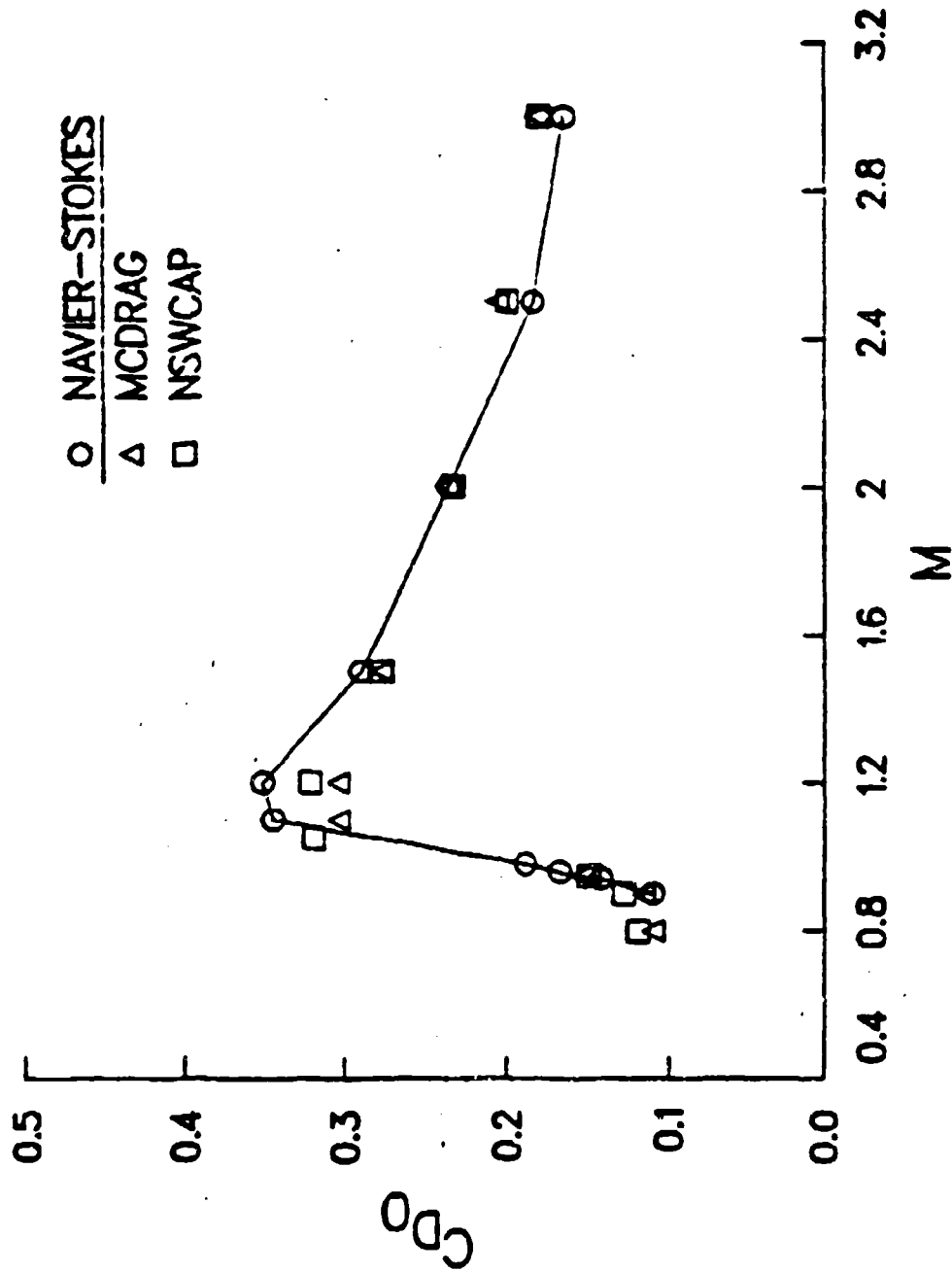
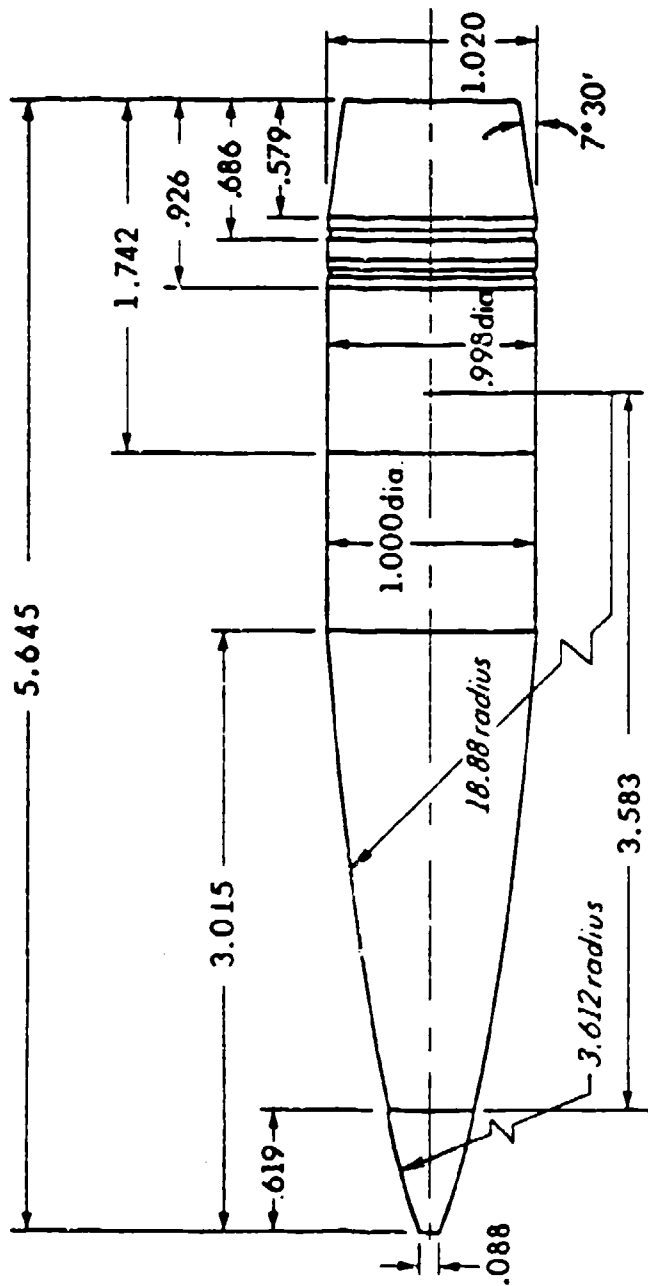


Figure 18. Variation of Total Drag Coefficient with Mach Number.
 $\alpha = 0$, SOCBI



155 mm, M549 PROJECTILE

- Wt. - 96.0 lbs
- I_P - 505.5 lb-in²
- I_T - 6610.0 lb-in²
- C.G. - 3.50 cal. from nose

NOTE:
Dimensions are in calibers

Figure 19. M549 Projectile

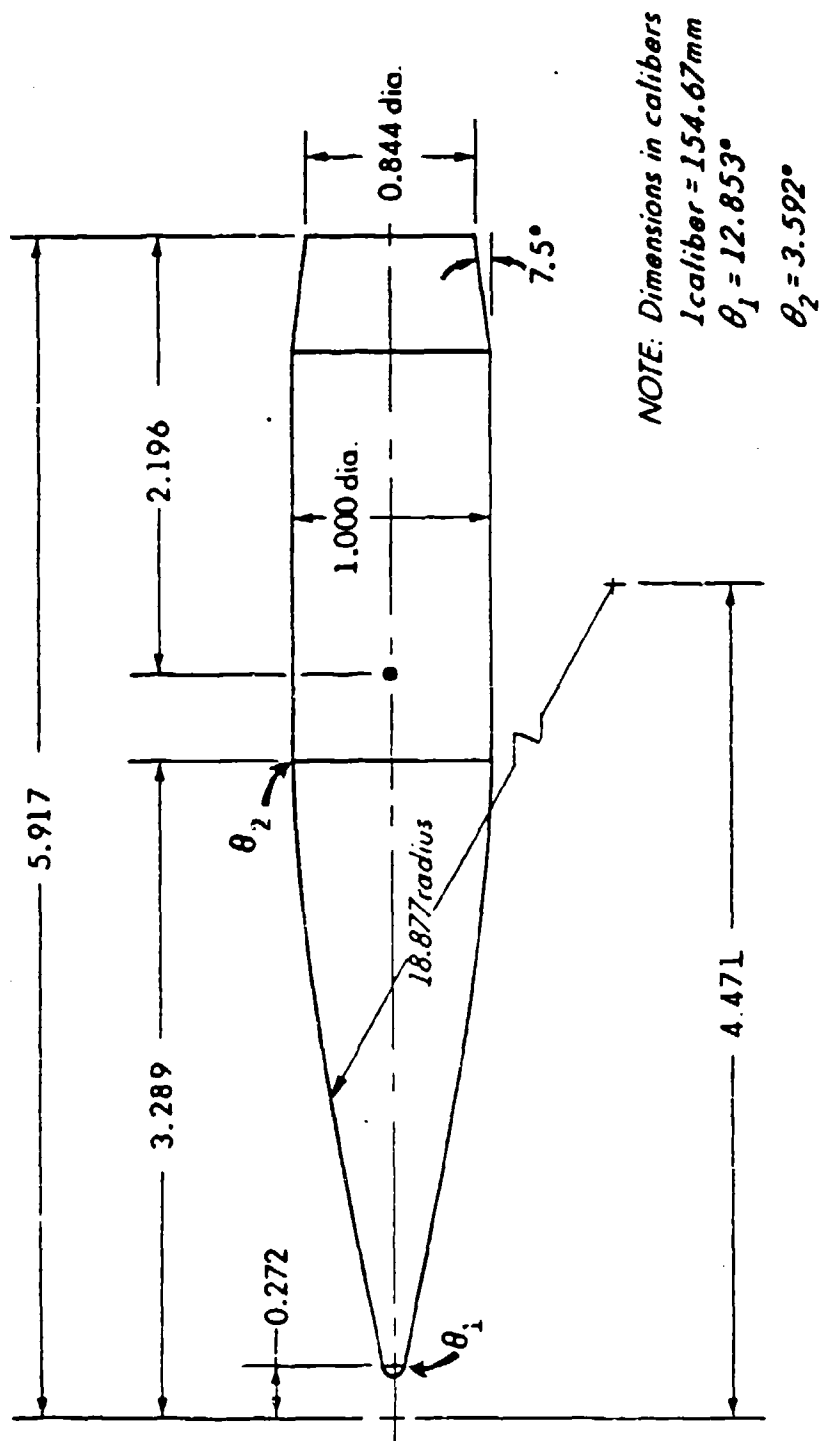


Figure 20. Computational Model

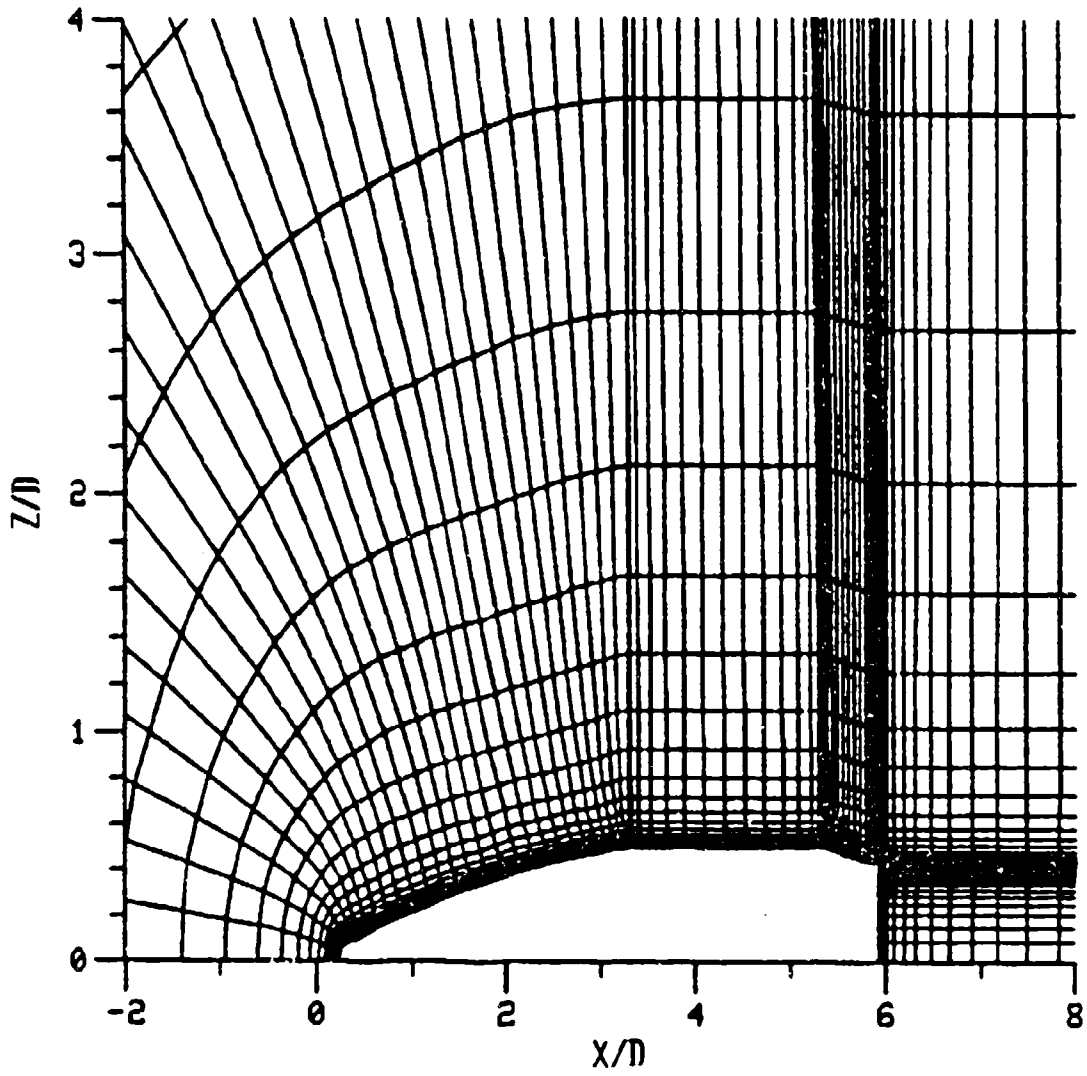


Figure 21. Physical Grid for M549 Projectile

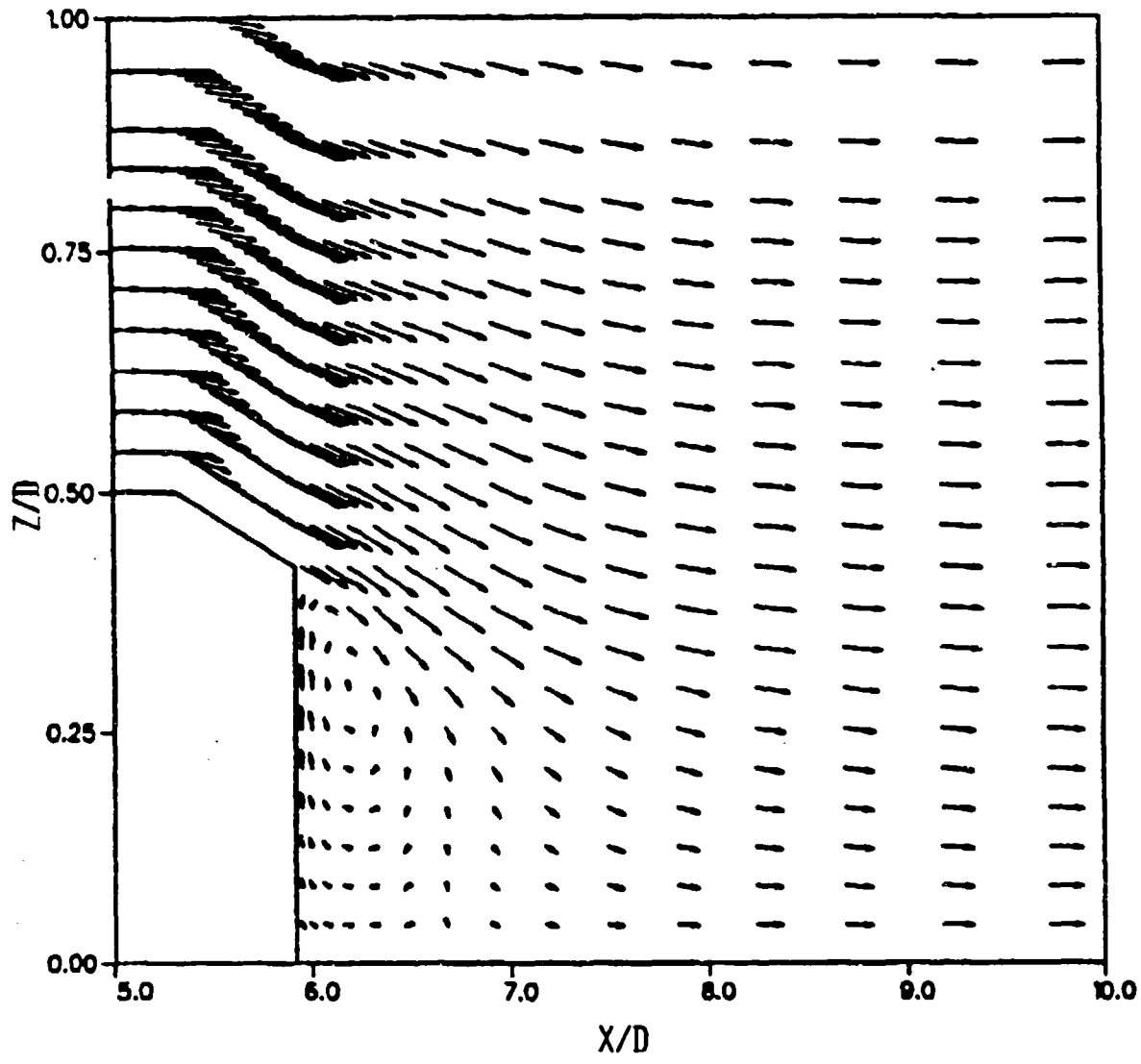


Figure 22. Velocity Vectors, $M_\infty = .9$, $\alpha = 0$, M549

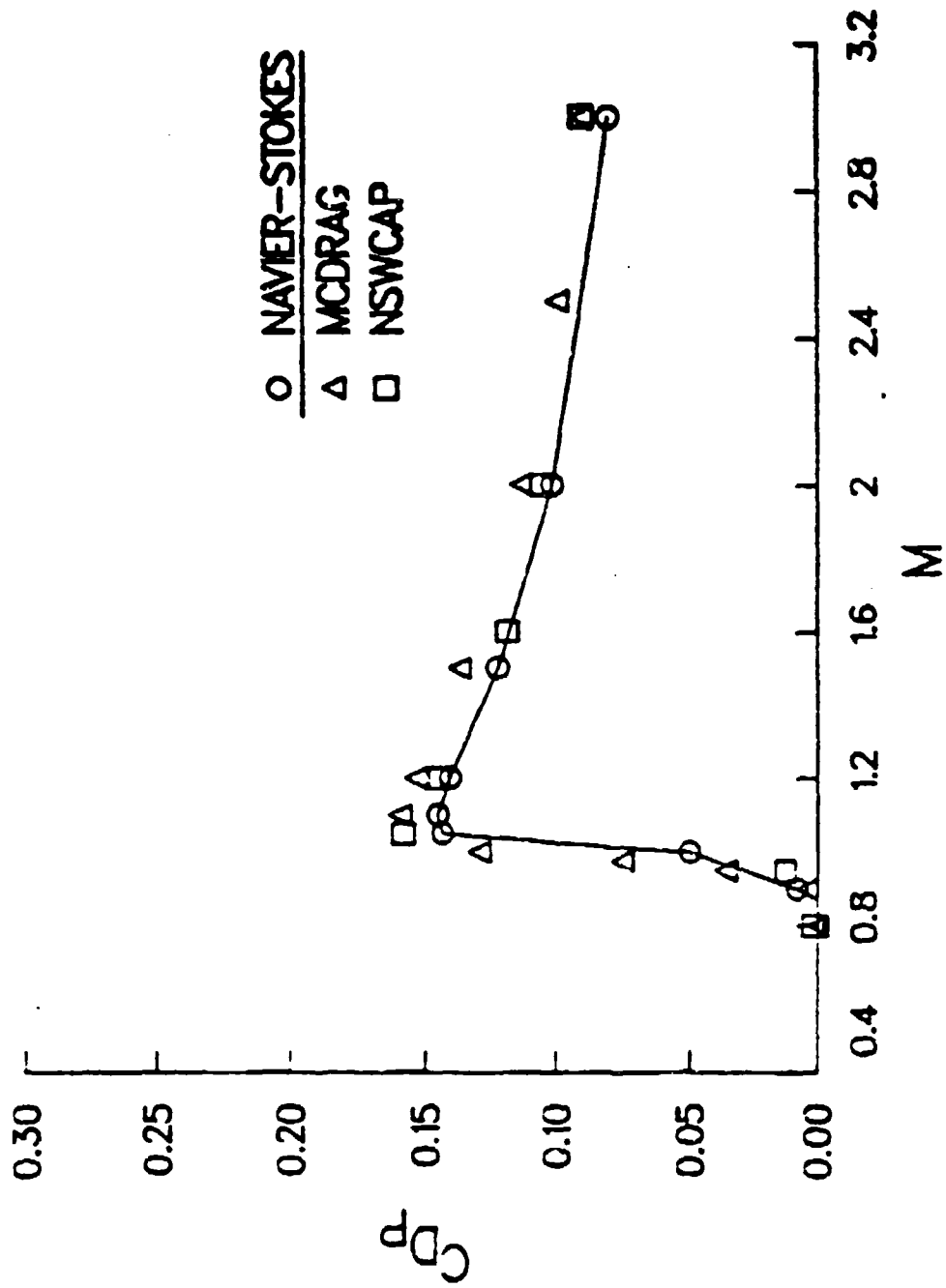


Figure 23. Pressure Drag Coefficient vs Mach Number, $\alpha = 0$, M549

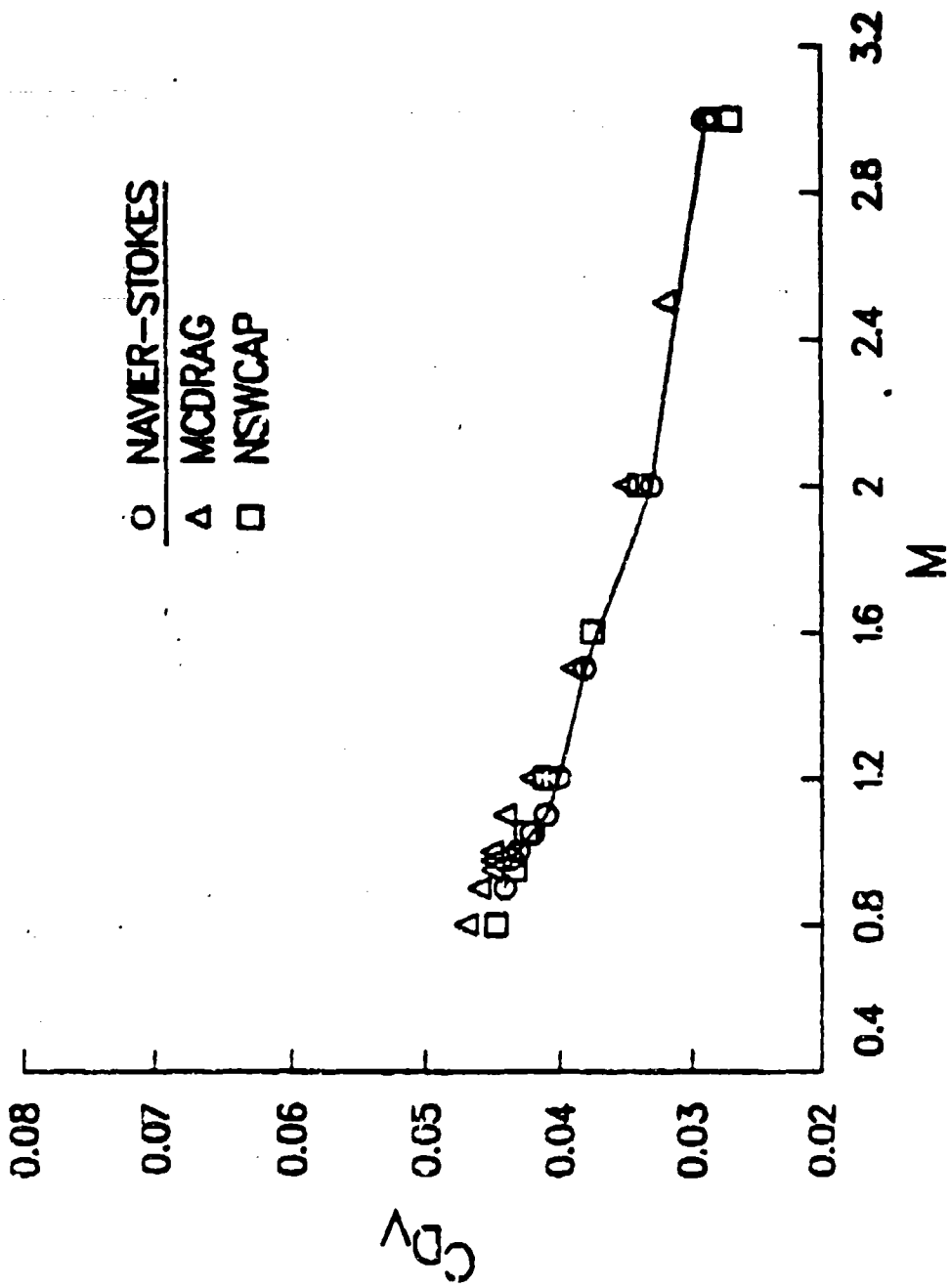


Figure 24. Viscous Drag Coefficient vs Mach Number, $\alpha = 0$, M549

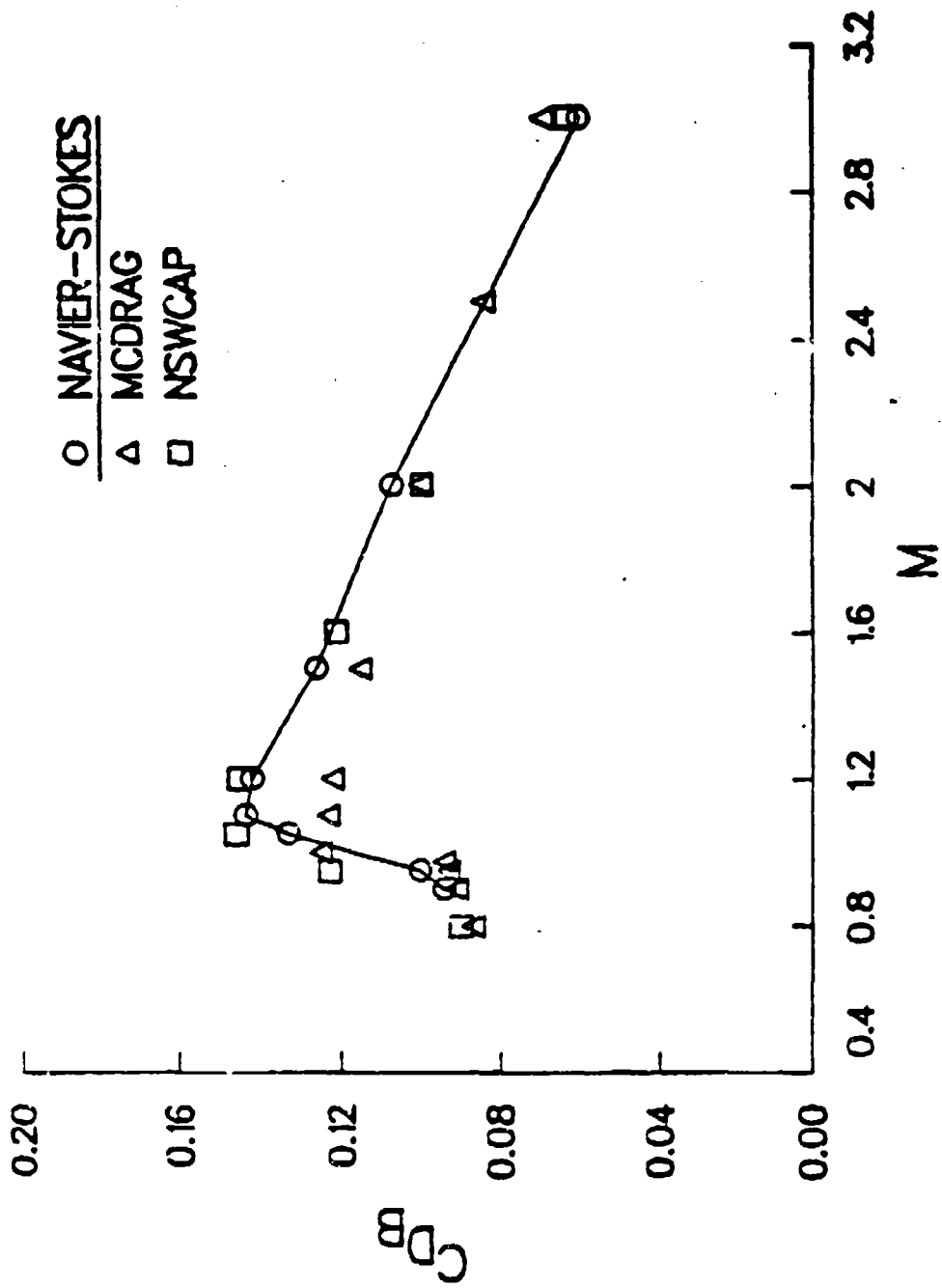


Figure 25. Base Drag Coefficient vs Mach Number, $\alpha = 0$, M549

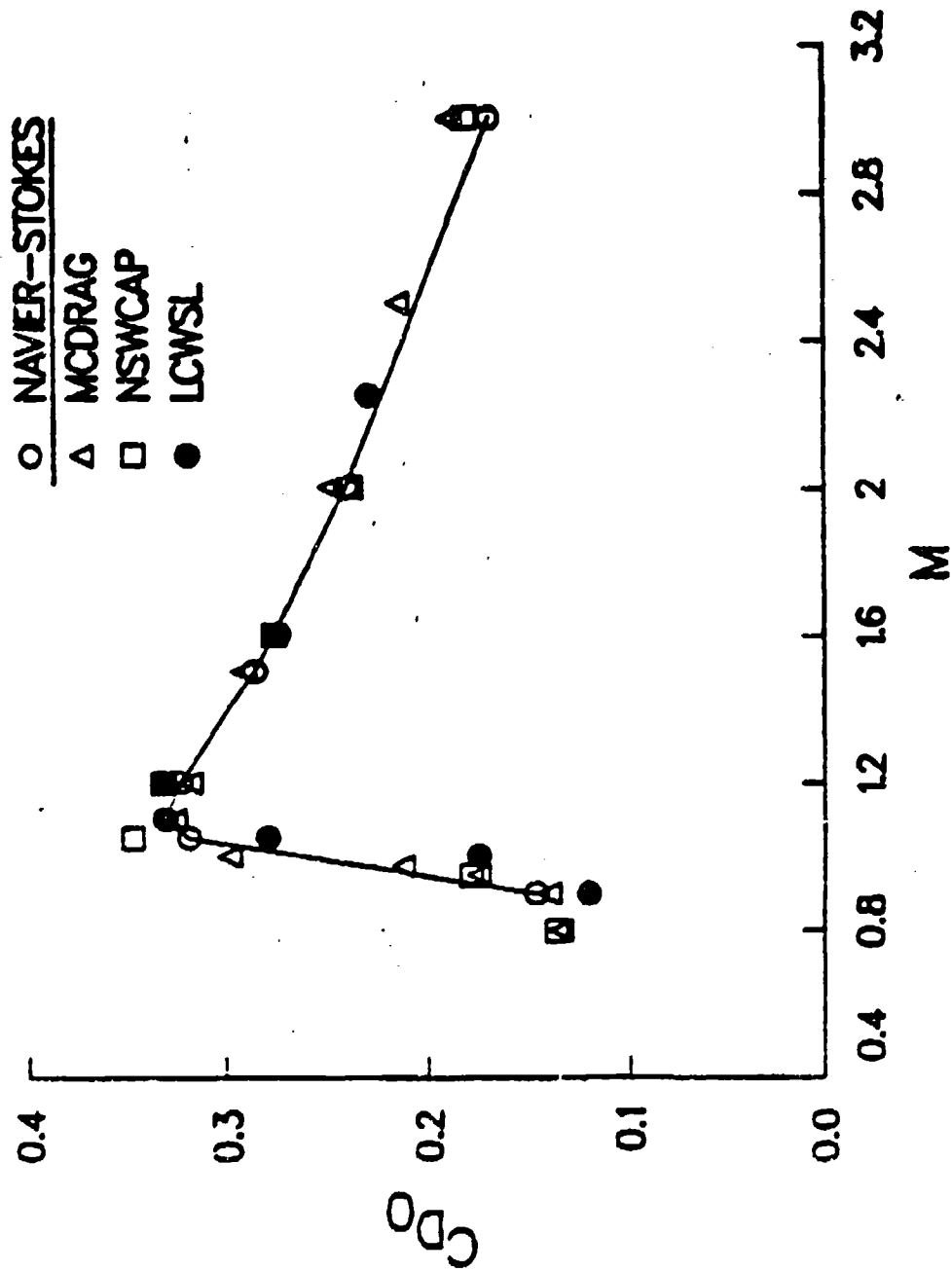


Figure 26. Total Drag Coefficient vs Mach Number, $\alpha = 0$, M549

REFERENCES

1. C.J. Nietubicz, T.H. Pulliam and J.L. Steger, "Numerical Solution of the Azimuthal-Invariant Navier-Stokes Equations," US Army Ballistic Research Laboratory, Aberdeen Proving Ground, Maryland, ARBRL-TR-02227, March 1980. (AD A085716) (Also see AIAA Journal, Vol. 18, No. 12, December 1980, pp. 1411-1412)
2. J.L. Steger, "Implicit Finite Difference Simulation of Flow About Arbitrary Geometries with Application to Airfoils," AIAA Journal, Vol. 16, No. 7, July 1978, pp. 679-686.
3. T.H. Pulliam and J.L. Steger, "On Implicit Finite-Difference Simulations of Three-Dimensional Flow," AIAA Journal, Vol. 18, No. 2, February 1980, pp. 159-167.
4. R. Beam and R.F. Warming, "An Implicit Factored Scheme for the Compressible Navier-Stokes Equations," AIAA Journal, Vol. 16, No. 4, April 1978, pp. 393-402.
5. B.S. Baldwin and H. Lomax, "Thin-Layer Approximation and Algebraic Model for Separated Turbulent Flows," AIAA Paper No. 78-257, 1978.
6. J. Sahu, C.J. Nietubicz and J.L. Steger, "Numerical Computation of Base Flow for a Projectile at Transonic Speeds," US Army Ballistic Research Laboratory, Aberdeen Proving Ground, Maryland, ARBRL-TR-02495, June 1983. (AD A130293) (Also see AIAA Paper No. 82-1358, August 1982)
7. J. Sahu, C.J. Nietubicz and J.L. Steger, "Navier-Stokes Computations of Projectile Base Flow with and without Base Injection," US Army Ballistic Research Laboratory, Aberdeen Proving Ground, Maryland, ARBRL-TR-02532, November 1983. (AD A135738) (Also see AIAA Journal, Vol. 23, No. 9, September 1985, pp. 1348-1355)
8. F.G. Moore and R.C. Swanson, "Aerodynamics of Tactical Weapons to Mach Number 3 and Angle-of-Attack 15°, Part I - Theory and Application," NSWC/DL TR-3584, February 1977.
9. F.G. Moore and R.C. Swanson, "Aerodynamics of Tactical Weapons to Mach Number 3 and Angle-of-Attack 15°, Part II - Computer Program and Usage," NSWC/DL TR-3600, March 1977.
10. M.J. Van Dykes, "The Similarity Rules for Second-Order Subsonic and Supersonic Flow," NACA Tech Note 3875, October 1956.
11. E.R. Van Driest, "Turbulent Boundary Layers in Compressible Fluids," Journal of the Aeronautical Sciences, Vol. 18, No. 3, 1951, pp. 145-160.
12. R.L. McCoy, "McDrag - A Computer Program for Estimating the Drag Coefficient of Projectiles," US Army Ballistic Research Laboratory, Aberdeen Proving Ground, Maryland, ARBRL-TR-02293, February 1981. (AD A098110)

REFERENCES (Continued)

13. L.D. Kayser, "Base Pressure Measurements on a Projectile Shape at Mach Numbers from 0.91 to 1.20," US Army Ballistic Research Laboratory, Aberdeen Proving Ground, Maryland, ARBRL-MR-03353, April 1984. (AD A141341)
14. P.R. Payne and R.M. Hartley, "Afterbody Drag, Volume 1 - Drag of Conical and Circular Arc Afterbodies without Jet Flow," Final Report, DTNSRDC/ASED-80-10, Bethesda, Maryland, May 1980.
15. L.D. Kayser, "Surface Pressure Measurements on a Boat-tailed Projectile Shape at Transonic Speeds," US Army Ballistic Research Laboratory, Aberdeen Proving Ground, Maryland, ARBRL-MR-03161, March 1982. (AD A113520)
16. A. Loeb, "Private Communication," Large Caliber Weapons Systems Laboratory, ARDC, AMCCOM, Dover, New Jersey.

DISTRIBUTION LIST

<u>No. of Copies</u>	<u>Organization</u>	<u>No. of Copies</u>	<u>Organization</u>
12	Administrator Defense Technical Info Center ATTN: DTIC-DDA Cameron Station Alexandria, VA 22304-6145	1	Director US Army Air Mobility Research and Development Command Ames Research Center Moffett Field, CA 94035
1	HQDA DAMA-ART-M Washington, DC 20310	1	Commander US Army Communications - Electronics Command ATTN: AMSEL-ED Fort Monmouth, NJ 07703
1	Commander US Army Materiel Command ATTN: AMCDRA-ST 5001 Eisenhower Avenue Alexandria, VA 22333-0001	1	Commander ERADCOM Technical Library ATTN: DELSD-L (Reports Section) Fort Monmouth, NJ 07703-5301
6	Commander Armament R&D Center US Army AMCCOM ATTN: SMCAR-TDC SMCAK-TSS SMCAR-LCA-F Mr. D. Mertz Mr. A. Loeb Mr. H. Hudgins Mr. E. Friedman Dover, NJ 07801	3	Commander US Army Missile Command Research, Development & Engineering Center ATTN: AMSMI-RD Dr. B. Walker Mr. R. Deep Redstone Arsenal, AL 35898-5500
	Commander US Army Armament, Munitions & and Chemical Command ATTN: SMCAR-ESP-L Rock Island, IL 61299	1	Director US Army Missile & Space Intelligence Center ATTN: AIAMS-YDL Redstone Arsenal, AL 35898-5500
1	Director Benet Weapons Laboratory Armament R&D Center US Army AMCCOM ATTN: SMCAR-LCB-TL Watervliet, NY 12189	1	Commander US Army Tank Automotive Command ATTN: AMSTA-TSL Warren, MI 48397-5500
1	Commander US Army Aviation Research and Development Command ATTN: AMSAV-E 4300 Goodfellow Blvd. St. Louis, MO 63120	1	Director US Army TRADOC Systems Analysis Activity ATTN: ATAA-SL White Sands Missile Range, NM 88002
		1	Commander US Army Research Office P. O. Box 12211 Research Triangle Park, NC 27709

DISTRIBUTION LIST

<u>No. of Copies</u>	<u>Organization</u>	<u>No. of Copies</u>	<u>Organization</u>
1	Commander US Naval Air Systems Command ATTN: AIR-604 Washington, D. C. 20360	1	Air Force Armament Laboratory ATTN: AFATL/DLODL Eglin AFB, FL 32542-5000
2	Commander US Naval Surface Weapons Center ATTN: Dr. T. Clare, Code DK20 Dr. F. Moore Dahlgren, VA 22448-5000	2	Director Sandia Laboratories ATTN: Division No. 1331, Mr. H.R. Vaughn Dr. F. Blottner P.O. Box 580 Albuquerque, NM 87184
1	Commander US Naval Surface Weapons Center ATTN: Dr. U. Jettmar Silver Spring, MD 20902-5000	1	AEDC Calspan Field Services ATTN: MS 600 (Dr. John Benek) AAFS, TN 37389
1	Commander US Naval Weapons Center ATTN: Code 3431, Tech Lib China Lake, CA 93555	1	Virginia Polytechnic Institute & State University ATTN: Dr. Clark H. Lewis Department of Aerospace & Ocean Engineering Blacksburg, VA 24061
1	Commander US Army Development and Employment Agency ATTN: MODE-TED-SAB Fort Lewis, WA 98433	1	University of California, Davis Department of Mechanical Engineering ATTN: Prof. H.A. Dwyer Davis, CA 95616
1	Director NASA Langley Research Center ATTN: NS-185, Tech Lib Langley Station Hampton, VA 23365	1	University of Delaware Mechanical and Aerospace Engineering Department ATTN: J.E. Danberg Newark, DE 19711
4	Director NASA Ames Research Center ATTN: MS-202A-14, Dr. P. Kutler MS-202-1, Dr. T. Pulliam Dr. J. Steger MS-227-8, Dr. L. Schiff Moffett Field, CA 94035	1	University of Florida Dept. of Engineering Sciences College of Engineering ATTN: Prof. C. C. Hsu Gainesville, FL 32611
2	Commandant US Army Infantry School ATTN: ATSH-CD-CSO-OR Fort Benning, GA 31905	1	University of Illinois at Urbana Champaign Department of Mechanical and Industrial Engineering ATTN: Prof. W. L. Chow Urbana, IL 61801

DISTRIBUTION LIST

<u>No. of Copies</u>	<u>Organization</u>
10	Central Intelligence Agency Office of Central Reference Dissemination Branch Room GE-47 HQS Washington, DC 20502
1	University of Maryland Department of Aerospace Engr. ATTN: Dr. J. D. Anderson, Jr. College Park, MD 20742
1	University of Notre Dame Department of Aeronautical and Mechanical Engineering ATTN: Prof. T. J. Mueller Notre Dame, IN 46556
1	University of Texas Department of Aerospace Engineering and Engineering Mechanics ATTN: Dr. D. S. Dolling Austin, Texas 78712-1055
	<u>Aberdeen Proving Ground</u>
	Dir, USAMSAA ATTN: AMXSU-D AMXSU-MP, H. Cohen
	Cdr, USATECOM ATTN: AMSTE-TO-F
	Cdr, CRDC, AMCCOM ATTN: SMCCR-RSP-A SMCCR-MU SMCCR-SPS-IL

USER EVALUATION SHEET/CHANGE OF ADDRESS

This Laboratory undertakes a continuing effort to improve the quality of the reports it publishes. Your comments/answers to the items/questions below will aid us in our efforts.

1. BRL Report Number _____ Date of Report _____

2. Date Report Received _____

3. Does this report satisfy a need? (Comment on purpose, related project, or other area of interest for which the report will be used.) _____

4. How specifically, is the report being used? (Information source, design data, procedure, source of ideas, etc.) _____

5. Has the information in this report led to any quantitative savings as far as man-hours or dollars saved, operating costs avoided or efficiencies achieved, etc? If so, please elaborate. _____

6. General Comments. What do you think should be changed to improve future reports? (Indicate changes to organization, technical content, format, etc.) _____

CURRENT ADDRESS

Name _____
Organization _____
Address _____
City, State, Zip _____

7. If indicating a Change of Address or Address Correction, please provide the New or Correct Address in Block 6 above and the Old or Incorrect address below.

OLD ADDRESS

Name _____
Organization _____
Address _____
City, State, Zip _____

(Remove this sheet along the perforation, fold as indicated, staple or tape closed, and mail.)